Perimeter Scholars International

Effective Edge States of Symmetry Protected Topological Systems

Jacob Bridgeman

Perimeter Scholars International 2013/2014

Perimeter Institute and University of Waterloo

Abstract

We use the group cohomology classification of (2+1)-dimensional symmetry protected topological states to construct explicit models for the gapless edges when the group is finite Abelian. We employ numerical techniques to investigate the properties of these models, identifying the CFTs associated to their thermodynamic description.

Acknowledgements

Contents

Chapter 1

Introduction

Studying interacting quantum systems and their thermodynamics is a major area of modern physics. The classification of both classical and quantum phases has allowed us to understand the underlying structure of quantum matter. It has led to deeper understanding of the role of entanglement in nature, and in turn to the discovery of emergent phenomena including particles with non-Abelian exchange statistics.

Recently, a new class of phases has discovered that lies outside the traditional framework. Some of these have exotic excitations and properties which cannot be changed by any local operation. In this essay, we will investigate models which capture some of the novel features of these systems.

In the second chapter, we will briefly review phases, both classical and quantum. We will discuss Landau's classification of phases, and the existence of phases that cannot be described in this way. We will introduce tensor networks as a means to argue for the classification of symmetry protected topological phases using group cohomology in both (1+1) and (2+1) dimensional systems.

In chapter three, we use constructions given in refs. [1, 2] to build explicit lattice models for the gapless edges of (2+1)-dimensional symmetry protected topological models where the symmetry is a finite Abelian group. We will also show how to construct models which have twisted boundary conditions.

In chapter four, we will describe two numerical methods which can be used to investigate the properties of gapless Hamiltonians. We will describe how to extract information about a conformal field theory associated with the thermodynamic limit of these models on both periodic and twisted boundaries.

In chapter five, we will employ these methods to learn about the lattice constructions. We will identify the associated CFTs and discover how the edges remain gapless in the presence of the symmetry. We will conclude by discussing some future work.

Chapter 2

Symmetry Protected Topological Order and Quantum Phases

Understanding phases and phase transitions has long been the focus of statistical and materials physics. The mid twentieth century saw the classification of classical phases using the concept of *symmetry breaking* and local order parameters [3]. In recent years, the ideas of *quantum phase transitions* and *topological phases* have arisen. These topological phases challenge the Landau paradigm; a new approach is required for their classification.

We begin this chapter with a brief review of Landau's scheme for describing phases and phase transitions in both the classical and quantum settings. We will then move on to describing phases beyond this paradigm by introducing topological phases. We will conclude by introducing symmetry protected topological (SPT) phases, which form the subject of the remainder of this document.

2.1 Symmetry Breaking Classification of Phases

The Landau classification of phases has been an extremely fruitful paradigm for the description of both thermal and quantum phases. We begin with a discussion of classical phase transitions.

2.1.1 Thermal Phase Transitions

The free energy of a classical system described by a Hamiltonian H at temperature T is given by

$$f = U - TS, \tag{2.1}$$

where U is the internal energy, and S is the entropy. A phase transition occurs when the free energy of the system becomes nonanalytic (in the thermodynamic limit) as parameters in the Hamiltonian are varied. A phase is a region in parameter space within which the free energy remains analytic. Landau realised that this type of phase transition can (usually) be classified by the presence or absence of symmetry breaking. We will use the (2D) Ising model to illustrate this classification. Let $s_i = \pm 1$ be a classical variable at site i of a (square) lattice. Let

$$H = -J \sum_{<i,j>} s_i s_j - h \sum_i s_i, \tag{2.2}$$

where $\sum_{<i,j>}$ denotes a sum over nearest neighbour sites. It is clear that this Hamiltonian with $h = 0$ has a global $\mathbb{Z}_2$ symmetry realised by sending $s_i \to -s_i$ at every site. We will call a symmetry of this type onsite, since the symmetry can be realised as the combined action of single site operators.

At high temperatures, the variables take uniformly random values, meaning that the local order parameter known as the magnetisation $m = \frac{1}{N} \sum_i \langle s_i \rangle$ vanishes. This is the 'symmetric phase', since the order parameter

has the same $\mathbb{Z}_2$ symmetry as the Hamiltonian. In the low temperature phase, the magnetisation (spontaneously) picks a particular value ± 1. The spin flip symmetry, whilst still present in the Hamiltonian, is not realised in the state.

The above argument does not work in one dimension, since the entropy increase due to adding a domain wall is larger than the energy penalty, so adding domain walls decreases the free energy. There is a general theorem which states that for Hamiltonians with short range interactions, there cannot be phase transitions at nonzero temperature in one dimension [4]. It is known that the quantum Ising model exhibits a phase transition at $T = 0$, which leads us to *quantum phase transitions*.

2.1.2 Quantum Phase Transitions

Although no phase transitions driven by thermal fluctuations can occur in one dimension, we can have transitions driven by quantum fluctuations. Quantum phase transitions occur at zero temperature, and are thus are associated with ground states. A usual definition of a quantum phase is a region in parameter space over which the ground state energy remains analytic in the thermodynamic limit. A phase transition occurs when the gap between the ground and first excited state closes in the $N \to \infty$ limit [5].

The canonical example of a quantum phase transition is that in the transverse field Ising model

$$H_{\text{Ising}} = -J \sum \left(\frac{h}{J} \sigma_j^X + \sigma_j^Z \sigma_{j+1}^Z \right). \tag{2.3}$$

In the $h \to \infty$ limit, we have the (unique) ground state

$$|\psi_\infty\rangle = |++++\dots+\rangle, \tag{2.4}$$

where

$$\sigma_j^X |\pm\rangle_j = \pm |\pm\rangle_j. \tag{2.5}$$

In the opposite limit, we have a pair of degenerate ground states

$$|\psi_{0,a}\rangle = |0000\dots0\rangle \qquad\qquad |\psi_{0,b}\rangle = |1111\dots1\rangle, \tag{2.6}$$

where

$$\sigma_j^Z |0\rangle_j = +|0\rangle_j, \qquad\qquad \sigma_j^Z |1\rangle_j = -|1\rangle_j, \tag{2.7}$$

The Ising Hamiltonian eqn. (2.3) commutes with the operator $S = \prod \sigma_j^X$, corresponding to a $\mathbb{Z}_2$ symmetry. In the ordered phase ($h \to 0$), the ground states spontaneously break this symmetry. In the disordered phase, the symmetry is respected in the ground state. This shows that some quantum phase transitions can be classified using Landau's symmetry breaking scheme.

2.2 Beyond Landau

In the 1970's, it was realised that symmetry breaking could not describe all phase transitions. There are examples of phase transitions in both the classical and quantum settings which do not break the symmetry.
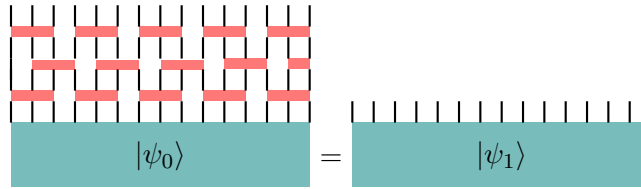
Figure 2.1 : Any two states which can be connected by a constant depth unitary circuit are said to be in the same phase.

2.2.1 Thermal Phases

The classical 2D XY model has a $U(1)$ symmetry, so by the theorem of Mermin and Wagner cannot have a symmetry breaking phase transition (no local order parameter) [6]. Despite this, it was realised that this classical model does support a thermal phase transition [7]. This was explained by Kosterlitz and Thouless by the introduction of vortices [8]. This is an arrangement of spins in the model which cannot be created by the action of local excitations. At the phase transition, vortices which were previously bound, and so carrying no net 'charge' become unbound. The 'charge' of a vortex can only be measured by a nonlocal operator (a closed loop around the vortex). These excitations are referred to a topological defects since they cannot be locally connected to the ground state.

2.2.2 Quantum Phases

Phases beyond Landau's classification also exist in the $T \rightarrow 0$ or quantum regime. We will work with these phases in this document, and begin with a precise definition of phases suitable for our purposes.

2.2.2.1 A Definition of Phases and Phase Transitions

We give two equivalent definitions of phases based on Ref. [9].

Given a pair of states $\{|\psi_0\rangle, |\psi_1\rangle\}$, these states are in the same phase if they can be connected using a local unitary evolution, or equivalently a constant (in system size) depth quantum circuit as shown in fig. 2.1. Notice that the operators act only on small blocks, irrespective of the system size. This is equivalent to evolution under a local Hamiltonian (local unitary evolution). If the states are separate when the local unitary circuits are picked only from a subgroup $\mathcal{S}$ of the full group of such transformations, we say the states are in distinct phases under $\mathcal{S}$

We expect phases to be stable under renormalisation, so we also insist that the phase cannot change under blocking sites together.

Another definition requires a pair Hamiltonians $\{H_0, H_1\}$ such that $\{|\psi_0\rangle, |\psi_1\rangle\}$ are the (gapped) ground states. If such a pair exists and there is also a continuous family H_λ such that the gap remains open for all $\lambda \in [0, 1]$, then $|\psi_0\rangle, |\psi_1\rangle$ are in the same phase (we also say that H_λ are in the same phase).

With this definition of phases, there is a clear link between the entanglement range and the phase. Short range entangled states can be disentangled into a product state using a local unitary evolution. As such, all short range entangled states are in the same phase if this definition is applied.

Topologically distinct phases are those whose states cannot be interconverted using any local unitary evolution. States which cannot be converted into the product state are said to be topologically nontrivial. There are many characteristic features present in topological phases of which two of the most interesting are protected ground state degeneracy and protected gapless excitation at the edge of a topological sample [10, 9, 11]. The ground state degeneracy is dependant on the underlying system. The Toric Code, for example, has four fold degeneracy if the lattice is placed on a torus, but a unique ground state if it is on a sphere. These ground spaces are robust to local perturbations, so are extremely interesting for quantum information storage [12, 13]. Some

topological phases also support anyonic excitations, which are interesting from both a quantum information processing [14] and developments in 'fundamental' physics [15].

We will not concern ourselves with topological order, but will focus on *symmetry protected topological order* (SPTO).
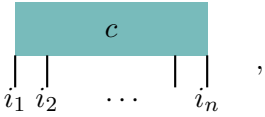
2.3 Symmetry Protected Topological Order

If we take the above definition of phases, all short range entangled (SRE) states belong to the same phase. We know, however, that different states and Hamiltonians possess different symmetries. It is natural then to ask what happens to this large SRE phase if certain symmetries are enforced on the unitaries allowed for the disentangling. It turns out that this causes the SRE phase to break up into subphases. The states in distinct SRE phases cannot be interconverted using *symmetric* local unitary evolution.

It is possible to find states in distinct SRE phases which do not spontaneously break the symmetry. These cannot be classified using Landau's scheme, a different property must be used to understand these symmetry protected topological phases.

SPT phases have properties similar to truly topological phases, including gapless edge excitations which are robust to *symmetry respecting* local perturbations. Nontrivial SPT states are thought to explain topological insulators (where the 'protecting' symmetry is time reversal) [16].

2.3.1 Classifying SPT phases

In this section we give a schematic argument, based on tensor networks, as to why SPT phases are classified using cohomology groups. This requires an understanding of the notation used for tensor network states. This will also be useful in section 4.2.

Tensor Networks

We focus on states which are defined on an n site lattice of d dimensional spins. This can be written as

$$|\psi\rangle = \sum_{i_1, i_2, \dots, i_n = 1}^{d} c_{i_1 i_2 \dots i_n} |i_1\rangle \otimes |i_2\rangle \cdots |i_n\rangle. \qquad (2.8)$$

Once a basis is fixed, all information about the state is stored in the exponentially large tensor $c_{i_1 i_2 \dots i_n}$. This can be drawn graphically as

$$(2.9)$$

where each leg corresponds to one of the indices. A matrix has two indices, so a matrix multiplication can be written as

$$A_a^b B_b^c = C_a^c \equiv \quad \begin{matrix} B \\ A \end{matrix} \quad = \quad C \quad , \qquad (2.10)$$

with any index connected to a pair of tensors being summed over.

Decomposing eqn. (2.9) by sequentially performing a singular value decomposition and only storing the χ largest singular values leads to the Matrix Product State ansatz.

$$
\begin{array}{c}
\boxed{c} \\
|\ |\ \cdots\ | \\
i_1\ i_2\ \ \ \ i_n
\end{array}
\ =\
\begin{array}{c}
\boxminus\!-\!\boxminus\!-\!\boxminus\!-\cdots-\!\boxminus\!-\!\boxminus
\end{array}
\ . \tag{2.11}
$$

Storage of the state in this form requires a number of coefficients *polynomial* in the number of sites. If we allow unbounded growth of the bond dimension, we can represent any state in the Hilbert space precisely. Clearly not all states can be represented exactly with polynomial bond dimension using this class of states, however the ground state of a gapped one dimensional spin chain can be approximated arbitrarily well with bond dimension χ only linear in n [17, 18]. We will use a simplified form of the MPS where the fully contracted tensors are absorbed into the tensors with free indices. Note that the MPS has a gauge freedom associated with choosing the basis on the bond or virtual indices. This can be used to bring the MPS into various standard forms.

$$
u - M - u^\dagger - u - M - u^\dagger - u - M - u^\dagger = M' - M' - M' \ . \tag{2.12}
$$

2.3.1.1 One Dimensional States-MPS and Projective Representations

Let $|\psi\rangle$ be the ground state of a one dimensional spin chain with local symmetry group $\mathcal{G}$, then

$$
U_g^{\otimes n}|\psi\rangle = |\psi\rangle \qquad \forall g \in \mathcal{G}, \tag{2.13}
$$

where U_g is a representation of $\mathcal{G}$. Suppose we have an MPS representation of the state, then we can use the gauge freedom to bring it into a form such that

$$
\begin{array}{c}
\boxed{} \\
\bullet \\
U_g
\end{array}
\ =\
V_g - \boxed{} - \bar{V}_g
\ , \tag{2.14}
$$

where the V_g are a *projective representation* of $\mathcal{G}$ [19]. Together $V_g \otimes \bar{V}_g$ form a linear representation.

Projective Representations

Given a group $\mathcal{G}$, a (linear) representation of $\mathcal{G}$ obeys

$$
U_g U_h = U_{gh} \qquad \forall g, h \in \mathcal{G}. \tag{2.15}
$$

A projective representation obeys

$$
V_g V_h = \omega[g, h] V_{gh} \qquad \forall g, h \in \mathcal{G}, \tag{2.16}
$$

---

where ω is a map from $\mathcal{G} \times \mathcal{G} \to U(1)$ called a 2-cocycle. By computing $V_{g_1} V_{g_2} V_{g_3} \to V_{g_1 g_2 g_3}$, it is clear that ω must obey

$$\frac{\omega[g_1, g_2 g_3] \omega[g_2, g_3]}{\omega[g_1 g_2, g_3] \omega[g_1, g_2]} = 1, \tag{2.17}$$

which is known as the 2-cocycle condition. The set of 2-cocycles for a group is known as a factor system. We might hope to remove all these $U(1)$ phases by rephasing (multiplying each V_g by a phase $\Omega[g]$) each V_g separately. We say that two factor systems are equivalent (so their projective representations are equivalent) if they are related by rephasing, so

$$\omega \equiv \omega' \iff \frac{\omega'[g, h]}{\omega[g, h]} = \frac{\Omega[gh]}{\Omega[g] \Omega[h]}. \tag{2.18}$$

This is known as a 2-coboundary.

The group of equivalence classes under the 2-coboundary condition is isomorphic to the second cohomology group $\mathcal{H}^2(G, U(1))$.

If we consider blocking sites together by multiplying their MPS tensors, we see that the projective representation on the edge of the block is left unchanged, so we say that the cohomology class is invariant under blocking. Suppose we have two states whose MPS tensors are in different cohomology classes, meaning that the projective representations are in different equivalence classes under local rephasing.

If we consider all the states which can be reached via a local unitary circuit commuting with U_g, it is clear that this must have the same cohomology class

$$\tag{2.19}$$
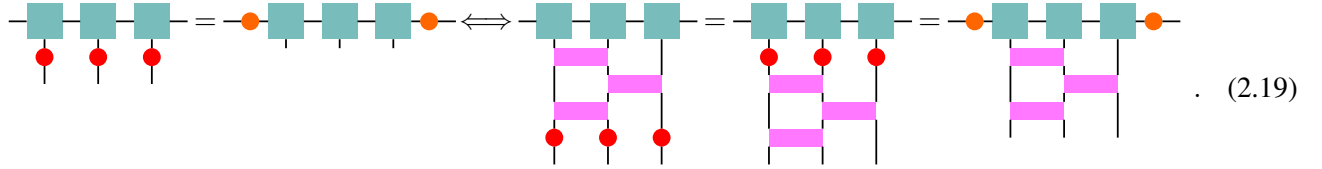
Thus, in one dimensional systems which do not break the symmetry, the phase can be identified by looking at how the MPS tensors transform under the symmetry. Each equivalence class of the projective representations of the symmetry group define one phase. The phases can then be labelled using the second cohomology group $\mathcal{H}^2(G, U(1))$.

2.3.1.2 Two Dimensional States-PEPS

Can the above classification scheme be used to identify phases in two dimensions? We will use the projected entangled pair state (PEPS) ansatz shown in fig. 2.2 to argue that it cannot. Although not as well understood as MPS, it can be shown that ground states have PEPS representations with bond dimension growing subexponentially [20, 21].

Assume that eqn. (2.14) generalises to

$$\tag{2.20}$$
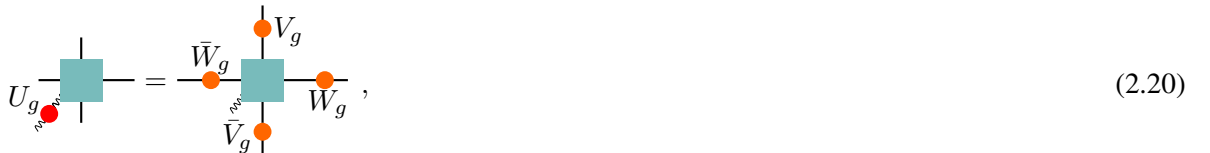
where V_g and W_g are projective representations. If we block sites together, we'll end up with tensor products of projective representations acting on the combined legs. Since this takes the product of the phases, it can change
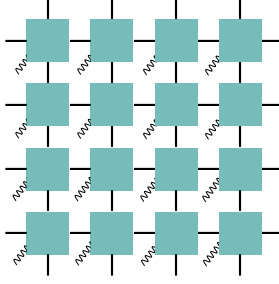
Figure 2.2 : The PEPS ansatz tensor network for two dimensional gapped states is the generalisation of the MPS. The physical indices are shown squiggly, with the straight indices being contracted.

the cohomology class. In particular, we can block sites and locally rephase to change the class to the trivial one. Thus, $\mathcal{H}^2(G, U(1))$ is not good for classifying two dimensional SPT systems; we need something else.

Here we schematically argue for the third cohomology group as being a possible classification of the SPT phases. For technical details, see ref. [10]. Suppose that when we push the symmetry through to the virtual indices it does not factorise into a tensor product of terms acting on each index separately. Suppose instead we end up with

$$(2.21)$$

where the contraction of the T_g around the loop forms a unitary representation of the symmetry group U'_g. The bond dimension of the T_g are not 1, so the symmetry cannot act on single sites. This decomposition of the operator is known as a matrix product operator (MPO).

Suppose we apply two symmetry transformations sequentially, then we want $T_g T_{gh} = T_{gh}$, however the bond dimension will have increased.

$$(2.22)$$

As such, we need to apply a projector (a map from $\mathbb{C}^\chi \times \mathbb{C}^\chi \to \mathbb{C}^\chi$) to the bond indices to bring it back to the correct form

$$(2.23)$$

If we apply more than two symmetry operators, we have a choice of which order to apply the projectors in. If we consider applying only the right projectors, these choices need to be the same up to a phase ϕ. If we apply

three operators, we have

$$= \phi[g_1, g_2, g_3] \qquad . \tag{2.24}$$

Now, in if we apply four in a row and consider how to project, we can derive a condition on these phases

$$= \phi[g_1, g_2, g_3] \qquad = \phi[g_1, g_2, g_3]\phi[g_1, g_2g_2, g_4]$$

$$= \phi[g_1, g_2, g_3]\phi[g_1, g_2g_3, g_4]\phi[g_2, g_3, g_4] \tag{2.25}$$

$$= \phi[g_1g_2, g_3, g_4]$$

$$= \phi[g_1g_2, g_3, g_4]\phi[g_1, g_2, g_3g_4] \tag{2.26}$$

$$\implies \frac{\phi[g_1, g_2, g_3]\phi[g_1, g_2g_3, g_4]\phi[g_2, g_3, g_4]}{\phi[g_1g_2, g_3, g_4]\phi[g_1, g_2, g_3g_4]} = 1, \tag{2.27}$$

which is known as the 3-cocycle condition. If we examine the projectors, we see that we can rephase each one without changing anything. In analogy to eqn. (2.18), we declare projectors equivalent if they are related in this way, so

$$\phi \equiv \phi' \iff \frac{\phi'[g_1, g_2, g_3]}{\phi[g_1, g_2, g_3]} = \frac{\omega[g_2, g_3]\omega[g_1, g_2g_3]}{\omega[g_1, g_2]\omega[g_1g_2, g_3]}, \tag{2.28}$$

known as a 3-coboundary.

This equivalence class is isomorphic to the third cohomology group $\mathcal{H}^3(G, U(1))$. If we consider a series of T_g contracted along the bond indices (corresponding to blocking sites), we see that the phase collected at the end upon projection will be invariant. Since local rephasing will not change the class, we cannot change the class using a finite depth unitary circuit.

From the above argument, we learn two things. Firstly, the (2+1)-dimensional SPT phases are labelled by $\mathcal{H}^3(G, U(1))$ if the symmetry action eqn. (2.21) was a correct assumption. We also see that the effective symmetry at the edge (associated with promoting bonds to physical indices around the boundary) will act in a non-onsite

manner. If we pick a bond dimension $\chi = 1$ on the MPO, we recover an onsite symmetry, corresponding to the trivial phase. In this chapter, we have briefly reviewed both classical and quantum phases. We have seen that

there are phases which are not described by symmetry breaking. By considering tensor network descriptions of symmetric ground states, we have argued that the SPT phases should be classified by the cohomology class of the effective symmetry at the edge. In (1+1) dimensions, this corresponds to the projective representation under which the edges transform. In (2+1) dimensions, the edge is protected by a non-onsite symmetry, with the phase being described by the 3-cocycles associated to this.

Chapter 3

Lattice Constructions for SPT Edge States

The edge of a 2D symmetry protected topological (SPT) state supports gapless boundary excitations. In chapter 2, we saw that the effective symmetry at the edge will act in a non-onsite manner. The gapless edge states are protected by this symmetry; its presence forbids the edge from being both gapped and symmetric. As such, we expect the effective edge model to either be gapless and symmetric, or to spontaneously break the symmetry.

In this chapter, we use the constructions given in refs. [1, 2] to build explicit models for the edge of SPT systems protected by finite Abelian symmetries. A more detailed derivation is presented in appendix B, including the Type I case.

3.1 Realising Effective Lattice Models for SPT Edges

Suppose we have a (2+1)-dimensional SPT model protected by a finite Abelian symmetry group $G \cong \prod_{j=1}^{m} \mathbb{Z}_{N_j}$. As discussed in chapter 2, we expect the effective symmetry at the edge to act in a non-onsite manner, by which we mean that it cannot be factorised into a tensor product of single site operators by symmetry respecting local unitaries or blocking of sites. We expect the symmetry to be realised via a unitary MPO acting on the edge. The MPO should be associated with 3-cocycles as discussed in section 2.3.1.2. The third cohomology group of a finite Abelian group is given by

$$\mathcal{H}^3(G, U(1)) = \prod_{1 \leq i \leq j \leq k \leq m} \mathbb{Z}_{N_i} \times \mathbb{Z}_{N_{ij}} \times \mathbb{Z}_{N_{ijk}}, \tag{3.1}$$

where $N_{ijk} = \gcd(N_i, N_j, N_k)$ [2]. It is known that there are three classes of 3-cocycles known as Type I,II,III corresponding to labels from $\mathbb{Z}_{N_i}$, $\mathbb{Z}_{N_{ij}}$ or $\mathbb{Z}_{N_{ijk}}$ respectively [22, 2]. As such, we expect there to be three distinct types of symmetries which can be realised at the edge. Here we assume the ansatz given in refs. [1, 2]. Note that a phase can have nontrivial Type I, II and III labels simultaneously.

The Type I class was considered in ref. [1], so we do not construct the edge model here. Since this has labels in $\mathbb{Z}_{N_i}$ in eqn. (3.1), it is minimally realised at the edge of a SPT system protected by a $\mathbb{Z}_N$ symmetry, in particular, $\mathbb{Z}_2$ and $\mathbb{Z}_3$ models were constructed. It was observed that these have gapless excitations and a symmetric ground state.

3.1.1 Type II Symmetries

Type II corresponds to labels coming from $\mathbb{Z}_{N_{ij}}$, so is minimally realised at the edge of a $\mathbb{Z}_{N_a} \times \mathbb{Z}_{N_b}$ SPT model. Following refs. [1, 2], we will construct a spin chain on M sites. At each site j, we place a $N_1 \times N_2$ dimensional Hilbert space acted on by $\mathbb{Z}_{N_1}$ ($\sigma_j^{\{1\}}, \tau_j^{\{1\}}$) and $\mathbb{Z}_{N_2}$ ($\sigma_j^{\{2\}}, \tau_j^{\{2\}}$) operators such that

$$\left(\sigma_j^{\{1\}}\right)^{N_1} = \left(\tau_j^{\{1\}}\right)^{N_1} = \mathbb{1}_j = \left(\sigma_j^{\{2\}}\right)^{N_2} = \left(\tau_j^{\{2\}}\right)^{N_2} \tag{3.2}$$

$$\sigma_j^{\{a\}}\tau_k^{\{b\}} = \omega_a^{\delta_{jk}\delta_{ab}}\tau_k^{\{b\}}\sigma_j^{\{a\}}, \tag{3.3}$$

where

$$\omega_a = \exp\left(\frac{2\pi i}{N_a}\right). \tag{3.4}$$

We can choose a basis in which the operators are represented by

$$\sigma^{\{a\}} = \begin{pmatrix} 1 & 0 & 0 & \cdots & & 0 \\ 0 & \omega_a & 0 & \cdots & & 0 \\ 0 & 0 & \omega_a^2 & \cdots & & 0 \\ 0 & 0 & 0 & \ddots & & 0 \\ 0 & 0 & 0 & \cdots & & \omega_a^{N_a-1} \end{pmatrix}, \qquad \tau^{\{a\}} = \begin{pmatrix} 0 & 0 & 0 & \cdots & 0 & 1 \\ 1 & 0 & 0 & \cdots & 0 & 0 \\ 0 & 1 & 0 & \cdots & 0 & 0 \\ 0 & 0 & 1 & \ddots & 0 & 0 \\ 0 & 0 & 0 & \cdots & 1 & 0 \end{pmatrix}. \tag{3.5}$$

For $\mathbb{Z}_2$, this recovers the Pauli operators

$$\sigma = Z = \begin{pmatrix} 1 & 0 \\ 0 & -1 \end{pmatrix}, \qquad \tau = X = \begin{pmatrix} 0 & 1 \\ 1 & 0 \end{pmatrix}, \tag{3.6}$$

whilst for $\mathbb{Z}_3$, we have

$$\sigma = \begin{pmatrix} 1 & 0 & 0 \\ 0 & e^{2\pi i/3} & 0 \\ 0 & 0 & e^{-2\pi i/3} \end{pmatrix}, \qquad \tau = \begin{pmatrix} 0 & 0 & 1 \\ 1 & 0 & 0 \\ 0 & 1 & 0 \end{pmatrix}. \tag{3.7}$$

The symmetry ansatz for the edge states is [1, 2]

$$S_{(N_1,N_2)}^{\{1\},(p_1,p_{12})} = \prod_{j=1}^{M} \tau_j^{\{1\}} \prod_{j=1}^{M} U_{j,j+1}^{\{1\},(p_1)} \prod_{j=1}^{M} V_{j,j+2}^{\{1\},(p_{12})}, \tag{3.8}$$

$$S_{(N_1,N_2)}^{\{2\},(p_2,p_{21})} = \prod_{j=1}^{M} \tau_j^{\{2\}} \prod_{j=1}^{M} U_{j,j+1}^{\{2\},(p_2)} \prod_{j=1}^{M} V_{j,j+2}^{\{2\},(p_{21})}, \tag{3.9}$$

where

$$U_{j,j+1}^{\{a\},(p_a)} = \exp\left(-\frac{2\pi i}{N_a^2}p_a \left\{\frac{N_a-1}{2} + \sum_{x=1}^{N_a-1} \frac{(\sigma_j^{\{a\}\dagger}\sigma_{j+1}^{\{a\}})^x}{\omega_a^x - 1}\right\}\right), \tag{3.10}$$

$$V_{j,j+2}^{\{a\},(p_{ab})} = \exp\left(-\frac{2\pi i}{N_a N_{ab}}p_{ab} \left\{\frac{N_{ab}-1}{2} + \sum_{x=1}^{N_{ab}-1} \frac{(\tilde{\sigma}_j^{\{b\}\dagger}\tilde{\sigma}_{j+2}^{\{b\}})^x}{\omega_{ab}^x - 1}\right\}\right), \tag{3.11}$$

and

$$\omega_{ab} = \exp\left(\frac{2\pi i}{N_{ab}}\right), \tag{3.12}$$

$$\tilde{\sigma}_j^{\{a\}}\tau_k^{\{b\}} = \omega_{ab}^{\delta_{jk}\delta_{ab}}\tau_k^{\{b\}}\tilde{\sigma}_j^{\{a\}}. \tag{3.13}$$

Here p_1, p_2 are Type I labels (so $p_1 \in \mathbb{Z}_{N_1}$ $p_2 \in \mathbb{Z}_{N_2}$), and p_{12}, p_{21} are of Type II (so $p_{12} \in \mathbb{Z}_{N_{1,2}}$). Note that the Type II operators V act on next nearest neighbour sites. This is to prevent cancellation of the Type I parts; if these are not present, the symmetry can be reduced to a nearest neighbour operator.

The ansatz Hamiltonian for the edge is given by constructing the symmetrisation of the τ operator acting on each site

$$H_{\vec{N}}^{(\vec{p})} = -\lambda \sum_{j=1}^{M} \sum_{\vec{a}=0}^{\vec{N}-1} \left(\vec{S}_{\vec{N}}^{(\vec{p})} \right)^{-\vec{a}} \vec{\tau}_j \left(\vec{S}_{\vec{N}}^{(\vec{p})} \right)^{\vec{a}} + hc \tag{3.14}$$

$$= -\lambda \sum_{j=1}^{M} \sum_{a_1=0}^{N_1-1} \sum_{a_2=0}^{N_2-1} \left(S_{(N_1,N_2)}^{\{1\},(p_1,p_{12})} \right)^{-a_1} \left(S_{(N_1,N_2)}^{\{2\},(p_2,p_{21})} \right)^{-a_2} (\tau_j^{\{1\}} + \tau_j^{\{2\}}) \times$$

$$\left(S_{(N_1,N_2)}^{\{1\},(p_1,p_{12})} \right)^{a_1} \left(S_{(N_1,N_2)}^{\{2\},(p_2,p_{21})} \right)^{a_2} + hc. \tag{3.15}$$

From here we will allow the $\vec{A}$ notation to be implied. With this, we can construct explicit Hamiltonians. Note that periodic boundary conditions are assumed at all times.

3.1.1.1 $\mathbb{Z}_2 \times \mathbb{Z}_2$ Symmetry

Since the case of Type I indices has already been considered, let $p_1 = p_2 = 0$. Let $p_{12} = 1$ to examine the nontrivial phase. It is then sufficient to let $p_{21} = 0$ [2]. With this symmetry, it is convenient to describe the Hilbert space as a pair of spin-1/2 degrees of freedom. As such, we use the Pauli operators ($\tau \to X$, $\sigma \to Z$) in the following. In this phase, we have the edge symmetry operators (reducing V to a nearest neighbour operator as discussed)

$$S^{\{1\}} = \prod_{j=1}^{M} X_j^{\{1\}} \prod_{j=1}^{M} V_{j,j+1}^{\{1\},(1)}, \tag{3.16}$$

$$= \prod_{j=1}^{M} X_j^{\{1\}} \prod_{j=1}^{M} \exp\left(-\frac{\pi i}{4} \left\{ 1 - Z_j^{\{2\}} Z_{j+1}^{\{2\}} \right\} \right). \tag{3.17}$$

The Hamiltonian is

$$H = -2\lambda \sum_{j=1}^{M} (X_j^{\{1\}} + X_j^{\{2\}}) +$$

$$\prod_{k=1}^{M} \exp\left(-\frac{\pi i}{4} Z_k^{\{2\}} Z_{k+1}^{\{2\}} \right) (X_j^{\{1\}} + X_j^{\{2\}}) \prod_{k=1}^{M} \exp\left(\frac{\pi i}{4} Z_k^{\{2\}} Z_{k+1}^{\{2\}} \right) \tag{3.18}$$

$$= -2\lambda \sum_{j=1}^{M} (2X_j^{\{1\}} + X_j^{\{2\}} - Z_{j-1}^{\{2\}} X_j^{\{2\}} Z_{j+1}^{\{2\}}). \tag{3.19}$$

On the $\{1\}$-subspace, this Hamiltonian has a unique gapped ground state. The Hamiltonian on the $\{2\}$-subspace is exactly that seen in the Type I case [1].

3.1.2 Type III Symmetries

The symmetry ansatz for the Type III case is very different from that for the Type I and II cases. A derivation is presented in [2] by first writing a field theoretic version, and regularising on a lattice. Here we take it as an ansatz. For simplicity, suppose that the Type I and II indices are trivial. Let $p_{1,2,3}$ be the only nontrivial index.

Since Type III labels come from $\mathbb{Z}_{N_{ijk}}$, they are minimally realised when the bulk symmetry is $\mathbb{Z}_{N_a} \times \mathbb{Z}_{N_b} \times \mathbb{Z}_{N_c}$. Placing a $N_a \times N_b \times N_c$ dimensional Hilbert space at each of the M sites on the chain as in the Type II

case, the edge symmetry is given by

$$S_{N_1}^{\{u\}} = \prod_{j=1}^{M} \tau_j^{\{u\}} \prod_{k=1}^{M} W_{k,k+1;N_u}^{\{u\}}, \tag{3.20}$$

where

$$W_{j,j+1;N_u}^{\{u\}} = \prod_{v,w=1}^{3} \left[\left(\sigma_j^{\{v\}} \right)^\dagger \sigma_{j+1}^{\{v\}} \right]^{\frac{N_v N_w}{i2\pi N_{uvw}} \epsilon_{uvw} p_{uvw} \log \sigma_j^{\{w\}}}. \tag{3.21}$$

3.1.3 $\mathbb{Z}_2 \times \mathbb{Z}_2 \times \mathbb{Z}_2$ Symmetry

Let us now specialise to the case of $\mathbb{Z}_2 \times \mathbb{Z}_2 \times \mathbb{Z}_2$ symmetry in the bulk. Pick the phase labelled by $p_\alpha = 0$ for $\alpha \neq 123$ and $p_{123} = 1$. In this phase, we end up with the boundary symmetry operators

$$S_2^{\{1\}} = \prod_{j=1}^{M} X_j^{\{1\}} \prod_{j=1}^{M} \left[Z_j^{\{2\}} Z_{j+1}^{\{2\}} \right]^{\frac{\log Z_j^{\{3\}}}{i\pi}}, \tag{3.22}$$

$$S_2^{\{2\}} = \prod_{j=1}^{M} X_j^{\{2\}}, \tag{3.23}$$

$$S_2^{\{3\}} = \prod_{j=1}^{M} X_j^{\{3\}}, \tag{3.24}$$

The ansatz Hamiltonian for this phase is therefore

$$H = -4 \sum_{j=1}^{M} (X_j^{\{1\}} + X_j^{\{2\}} + X_j^{\{3\}}) + \left(S_2^{\{1\}} \right)^{-1} (X_j^{\{1\}} + X_j^{\{2\}} + X_j^{\{3\}}) \left(S_2^{\{1\}} \right) \tag{3.25}$$

$$= -4 \sum_{j=1}^{M} (2X_j^{\{1\}} + X_j^{\{2\}} + X_j^{\{3\}}) + Z_{j-1}^{\{3\}} X_j^{\{2\}} Z_j^{\{3\}} + Z_j^{\{2\}} X_j^{\{3\}} Z_{j+1}^{\{2\}}. \tag{3.26}$$

Identifying the 2 and 3 subspaces as odd and even sites on a single chain, we get

$$H_{\text{TypeIII}} \equiv -8 \sum_{j=1}^{M} X_j^{\{1\}} - 4 \sum_{j=1}^{2M} \tilde{X}_j + \tilde{Z}_{j-1} \tilde{X}_j \tilde{Z}_{j+1}, \tag{3.27}$$

which can be compared to the Type II Hamiltonian

$$H_{\text{TypeII}} = -2 \sum_{j=1}^{M} (2X_j^{\{1\}} + X_j^{\{2\}} - Z_{j-1}^{\{2\}} X_j^{\{2\}} Z_{j+1}^{\{2\}}). \tag{3.28}$$

3.1.4 Twisted Boundary Conditions

In addition to the edge models constructed above, all of which exist on a periodic lattice, it is interesting to consider the effect of twisted boundary conditions. In the field theoretic limit, this corresponds to insertion of a gauge flux through the ring. The effect of this is a kind of Aharonov-Bohm effect [1]. These effective edge Hamiltonians may remain gapless, but have spectra shifted with respect to the untwisted constructions.

3.1.4.1 Ising Model

To describe the construction, we use the Ising model as an example. The Hamiltonian for the periodic Ising model is

$$H = -\sum_{j=1}^{M} X_j - \sum_{j=1}^{M-1} Z_j Z_{j+1} - Z_M Z_1 \tag{3.29}$$

$$= -\sum_{j=1}^{M} h_j, \quad \text{where} \quad h_j = X_j + Z_j Z_{j+1}. \tag{3.30}$$

The symmetry operator of this model is $S = \prod_{j=1}^{N} X_j$. The translation operator acts as $T^\dagger o_j T = o_{j+1}$, where o_j is an operator at site j. Clearly the above Hamiltonian is translationally invariant. Define the 'twisted translation operator'

$$\tilde{T} = T X_1. \tag{3.31}$$

Let us construct a Hamiltonian which commutes with this operator instead of T. Then we can see that most terms already commute with the X_1. We want $\tilde{h}_{j+1} = \tilde{T}^\dagger h_j \tilde{T}$. Leaving h_{M-1} invariant, we can construct

$$\tilde{h}_M = X_1 T^\dagger (X_{M-1} + Z_{M-1} Z_M) T X_1 \tag{3.32}$$

$$= X_1 (X_M + Z_M Z_1) X_1 \tag{3.33}$$

$$= (X_M - Z_M Z_1) \tag{3.34}$$

$$\tilde{h}_1 = (X_1 + Z_1 Z_2). \tag{3.35}$$

This is nothing but the Ising model on antiperiodic boundary conditions.

3.1.5 Type II-$\mathbb{Z}_2 \times \mathbb{Z}_2$ Symmetry

In analogy to the Ising model above, we define the twisted translation operator in the above phase by

$$\tilde{T}^{(p)} = T V_{M,1}^{\{1\},(1)} X_1^{\{1\}}. \tag{3.36}$$

The untwisted Hamiltonian is given by

$$H = -2\lambda \sum_{j=1}^{M} (2X_j^{\{1\}} + X_j^{\{2\}} - Z_{j-1}^{\{2\}} X_j^{\{2\}} Z_{j+1}^{\{2\}}). \tag{3.37}$$

$$= -2\lambda \sum_{j=1}^{M} h_j. \tag{3.38}$$

As above, we can see that most terms will remain unchanged when the new translation operator is introduced. We compute the terms that are changed

$$\tilde{h}_M = \left(X_1^{\{1\}}\right)^\dagger \left(V_{M,1}^{\{1\},(1)}\right)^{-1} T^\dagger (2X_{M-1}^{\{1\}} + X_{M-1}^{\{2\}} - Z_{M-2}^{\{2\}} X_{M-1}^{\{2\}} Z_M^{\{2\}}) T V_{M,1}^{\{1\},(1)} X_1^{\{1\}} \tag{3.39}$$

$$= 2X_M^{\{1\}} + (Y_M^{\{2\}} Z_1^{\{2\}} - Z_{M-1}^{\{2\}} Y_M^{\{2\}}), \tag{3.40}$$

where Y is the Pauli Y operator $Y = iXZ$.

$$\tilde{h}_1 = \exp\left(-\frac{\pi i}{4} Z_M^{\{2\}} Z_1^{\{2\}}\right) (2X_1^{\{1\}} + Y_1^{\{2\}} Z_2^{\{2\}} - Z_M^{\{2\}} Y_1^{\{2\}}) \exp\left(\frac{\pi i}{4} Z_M^{\{2\}} Z_1^{\{2\}}\right) \tag{3.41}$$

$$= h_1, \tag{3.42}$$

so the only term which changes is

$$\tilde{h}_M = 2X_M^{\{1\}} + (Y_M^{\{2\}} Z_1^{\{2\}} - Z_{M-1}^{\{2\}} Y_M^{\{2\}}). \tag{3.43}$$

This term clearly breaks the original symmetry protecting the system.

3.1.5.1 Type III-$\mathbb{Z}_2 \times \mathbb{Z}_2 \times \mathbb{Z}_2$ Symmetry

We define the twisted translation operator in the above phase by

$$\tilde{T}^{(p)} = T\, W_{M,1}^{\{1\},(1)} X_1^{\{1\}}. \tag{3.44}$$

As before, we compute the terms which might change.

$$\tilde{h}_M = \left(X_1^{\{1\}} \right) \left(W_{M,1}^{\{1\},(1)} \right)^{-1} T^\dagger (2X_{M-1}^{\{1\}} + X_{M-1}^{\{2\}} + X_{M-1}^{\{3\}}$$
$$+ Z_{M-2}^{\{3\}} X_{M-1}^{\{2\}} Z_{M-1}^{\{3\}} + Z_{M-1}^{\{2\}} X_{M-1}^{\{3\}} Z_M^{\{2\}}) T W_{M,1}^{\{1\},(1)} X_1^{\{1\}} \tag{3.45}$$
$$= 2X_M^{\{1\}} + X_M^{\{2\}} Z_M^{\{3\}} + Z_{M-1}^{\{3\}} X_M^{\{2\}} + Z_M^{\{2\}} X_M^{\{3\}} Z_1^{\{2\}} + X_M^{\{3\}} \tag{3.46}$$
$$\tilde{h}_1 = X_1^{\{1\}} \left(W_{M,1}^{\{1\},(1)} \right)^{-1} T^\dagger (2X_M^{\{1\}} + X_M^{\{3\}} + X_M^{\{2\}} Z_M^{\{3\}} +$$
$$Z_{M-1}^{\{3\}} X_M^{\{2\}} + Z_M^{\{2\}} X_M^{\{3\}} Z_1^{\{2\}}) T W_{M,1}^{\{1\},(1)} X_1^{\{1\}} \tag{3.47}$$
$$= 2X_1^{\{1\}} + X_1^{\{2\}} + X_1^{\{3\}} + Z_1^{\{2\}} X_1^{\{3\}} Z_2^{\{2\}} + Z_M^{\{3\}} X_1^{\{2\}} Z_1^{\{3\}} \tag{3.48}$$
$$= h_1. \tag{3.49}$$

Thus, we have the Type III Hamiltonian for $\mathbb{Z}_2 \times \mathbb{Z}_2 \times \mathbb{Z}_2$ with a gauge flux.

We can write an new symmetry $\tilde{S}$ for the above models by letting $\tilde{S} = \tilde{T}^M$.

In this section, we have used the constructions given in refs. [1, 2] to build explicit Hamiltonians for the edge of SPT models protected by finite Abelian groups. We have constructed models where the effective edge symmetry corresponds to 3-cocycles of the two types which have not previously been investigated. Further, we have constructed models which corresponds to lattice models on twisted boundary conditions, or field theories with a nonzero gauge flux. In chapter 5, we will investigate the properties of these models. In particular, we will see that they correspond to $c = 1$ CFTs whose left and right movers transform differently under the symmetry, so protecting the gapless nature of the models.

Chapter 4

Numerical Methods for Gapless Hamiltonians

Classical simulation of many body quantum systems is typically believed to be a hard problem [23, 24]. The exponential growth of the Hilbert space in the system size hinders our understanding of strongly correlated systems. Despite this, a number of algorithms have proven effective in tackling quantum spin systems and quantum field theories even in the thermodynamic limit [25, 26, 27, 28, 29]. These generally take advantage of a property of low lying states known as the area law for entanglement entropy. Proven in one dimension [18] and widely believed in higher, this states that for the ground state of gapped systems, the correlations between a region B and the rest of a system scales like the area of B rather than it's volume. This special property leads to discussion of the 'physical corner' of Hilbert space. If we can simulate states with this restricted entanglement, maybe we can make progress.

At the edge of SPT systems, we expect either gapped symmetry breaking states or gapless symmetric states. If the edge modes are gapless, they do not obey the area law for entanglement entropy, and so are not directly amenable to the simulation techniques above. In this section, we describe exact diagonalisation of gapless models and the Multiscale Entanglement Renormalisation Ansatz (MERA). These techniques will be applied to examine the edge models constructed in chapter 3. Benchmarking results are included in appendix A.

4.1   Exact Diagonalisation for Gapless Hamiltonians

The most naive way to investigate the low energy states of a Hamiltonian is via exact diagonalisation (ED). Due to the exponentially fast growth of the Hilbert space, only chains of a few spins can be tackled (typically only 10-20). Since we are interested in thermodynamic properties (scaling dimensions), we will be making large extrapolations. Despite this, ED can be a very useful method if finite size effects are sufficiently small.

Our ED algorithm (based on that presented in [30]) uses the power method to find the ground state. This is achieved by initialising a random state. The Hamiltonian is shifted such that the spectrum is negative semidefinite, ensuring that the ground state has the largest magnitude eigenvalue. Applying the Hamiltonian to this random state and renormalising suppresses the higher energy states, and after many iterations the ground state is reached. The convergence is complete when the change in the state (measured using the fidelity) drops below a threshold (typically 10^{-10} in our implementation).

Once the ground state has been reached, other states can be found by projecting onto the orthogonal subspace after every application of the Hamiltonian. Our algorithm also projects onto given symmetry sectors, ensuring each state transforms properly under the symmetry.

Once all states of a given energy within one symmetry sector (± 1 under each $\mathbb{Z}_2$) have been found (typically between two and four for our models), the momentum can be calculated by constructing the appropriate subblock of the translation operator and diagonalising.

Exact Diagonalisation Algorithm

$$|\psi_j\rangle \rightarrow \frac{H|\psi_j\rangle}{||H|\psi_j\rangle||} \tag{4.1}$$

$$|\psi_j\rangle \rightarrow \frac{|\psi_j\rangle - \sum_{i<j} |\psi_i\rangle \langle\psi_i|\psi_j\rangle}{|| |\psi_j\rangle - \sum_{i<j} |\psi_i\rangle \langle\psi_i|\psi_j\rangle ||} \tag{4.2}$$

$$|\psi_j\rangle \rightarrow \frac{\prod_{i=1}^{n_s} \sum_{j=0}^{1} q_i^j S_i^j |\psi\rangle}{|| \prod_{i=1}^{n_s} \sum_{j=0}^{1} q_i^j S_i^j |\psi\rangle ||}, \tag{4.3}$$

where n_s is the number of $\mathbb{Z}_2$ symmetry operators. Given the translation operator T such that $T^\dagger o_j T = o_{j+1}$ for an operator o_j,

$$T_B = \sum_{i,j} \langle\psi_i|T|\psi_j\rangle. \tag{4.4}$$

gives the subblock of the translation operator when the sum is taken over the subspace of degenerate states with the same symmetry quantum number. Diagonalising this gives the eigenstates with definite momentum k defined by

$$T|\psi_k\rangle = e^{\frac{2\pi i}{M}k} |\psi_k\rangle. \tag{4.5}$$

One could project onto particular values of the momentum in the same way as eqn. (4.3), however we find that it is faster to use the algorithm above.

In applying the Hamiltonian, we make use of the fact that it is given by a sum of local terms

$$H = -\lambda \sum_{j=1}^{N} h_j, \tag{4.6}$$

where each h_j acts only on a few neighbouring terms. By applying each h_j separately, the ED algorithm can be implemented with time scaling like $\mathcal{O}(d^M)$, where d is the dimension of the spins and M is the number of spins on the (periodic) chain.

4.1.1 Conformal Data from ED

By scaling the Hamiltonian properly, one can compute the scaling dimensions of the CFT describing the thermo-dynamic limit of the critical spin chain up to finite size effects [31, 32]. Using the known scaling of entanglement entropy for one dimensional ground states

$$S = \frac{c}{3} \log(L) + k, \tag{4.7}$$

one can also compute the central charge c of the associated CFT.

4.2 Multiscale Entanglement Renormalisation Ansatz

The MERA is a tensor network ansatz designed primarily for the efficient description of ground states of spin chains [33, 34, 35], as well as the efficient computation of correlation functions. It describes a d dimensional state
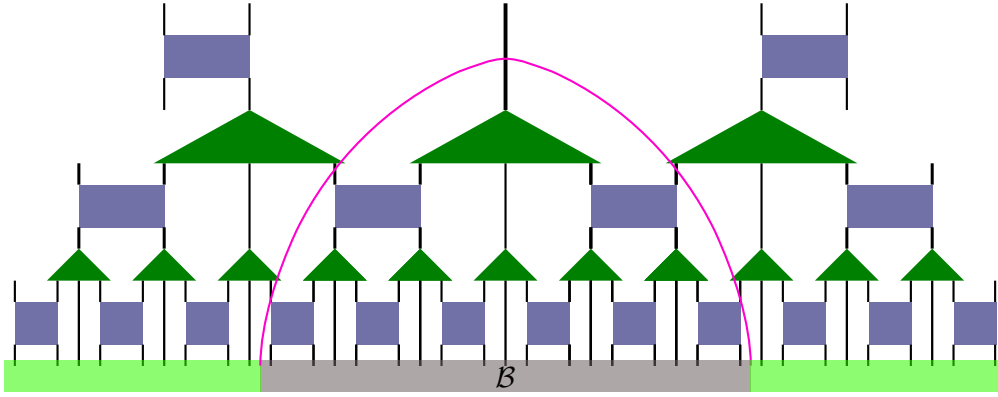
Figure 4.1 : The MERA is a tensor network ansatz for gapless states in one spacial dimension. It uses a second 'holographic' dimension to encode length scale and allow it to capture logarithmic violations of the area law, as seen in gapless states/conformal field theories. An entanglement cut is shown; the MERA can capture logarithmic violations of the area law.

using a $d+1$ dimensional network. This allows representation of states which violate the area law logarithmically, including the 1D gapless edge states at the boundary of a 2D SPT sample [36, 37].

A MERA network is shown in fig. 4.1. This is the ternary or $3:1$ MERA. Although other choices can be made, our implementation and discussion use this scheme. We review the MERA following ref. [34].

The ansatz is built from two kinds of tensors: $3:1$ isometric tensors w and $2:2$ unitaries u. To ensure that physical quantities such as correlation functions can be evaluated efficiently, the tensors obey the following constraints

$$\text{(4.8)}$$

The MERA has a clear layered structure. We interpret the free indices at the base as corresponding to a description of the system on the microscopic level. The isometries perform a rescaling operation, blocking sites and projecting out degrees of freedom. This gives an effective site of dimension χ, where χ is known as the bond dimension. The unitaries rearrange the local degrees of freedom, disentangling a block from its neighbours. Reducing the short range entanglement in this way allows the truncated Hilbert space to have a much smaller dimension [33].

The effect of these tensors is to perform a real space entanglement renormalisation group transformation. Each layer represents the system at a different length scale. Given a translationally invariant Hamiltonian, we can make all tensors in a given layer identical. If the Hamiltonian is also scale invariant (as is the case for a critical Hamiltonian) we can make each layer identical. Since the MERA is a state ansatz, the state is then completely characterised by a bond dimension χ and a pair of tensors $\{u, w\}$. Given a local Hamiltonian, we can optimise these tensors to best represent the ground state using a variational algorithm. The scheme we have used is based on that presented in ref. [34].

In tensor network states, it is easy to place an upper bound on the bipartite entanglement that can be captured. Given a region $\mathcal{B}$, the maximum amount of entanglement (measured using the von Neumann entropy for example) that can be represented is proportional to the number of bonds that must be cut to detach the region from the rest of the system. An entanglement cut for MERA is shown in fig. 4.1. The number of layers we must go up is proportional to the logarithm of the block size, so

$$S(\mathcal{B}) \leq a \log(|\mathcal{B}|), \tag{4.9}$$
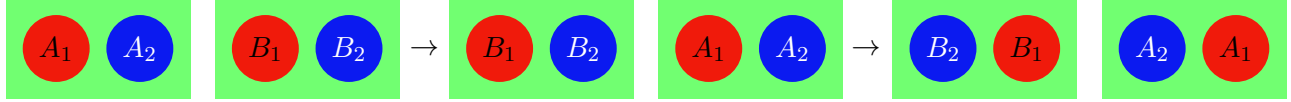
Figure 4.2 : If each site (green) contains multiple subsystems (red and blue), a reflection is more than just a reordering of sites. First we reorder the sites, then perform a unitary rotation within each site. The combined operation realises a spacial reflection.

allowing the MERA to capture the scaling expected in gapless one dimensional ground states.

4.2.1 Reflection Symmetric MERA

If the Hamiltonian of interest is symmetric under spacial reflections, it can be useful to incorporate this into the MERA. Here we explain how this is achieved following refs. [38, 39].

Reflection symmetry in the MERA is achieved by ensuring that each tensor is invariant under spacial reflection, so

$$w = R(w) \qquad\qquad u = R(u), \tag{4.10}$$

where R enacts a spacial reflection. It is important to carefully consider the action of this superoperator. Clearly it will perform a permutation of the indices of each tensor. It has an additional action; a unitary rotation on each index.

We want the tensors to have the property that

where r enacts the onsite rotation. We cannot simply symmetrise the tensors by

$$w \to \frac{1}{2}\left(w + R(w)\right), \tag{4.12}$$

since we will lose the property eqn. (4.8). We instead symmetrise the 'environment' of the tensors which is used within the update step. For example, one of the environments of u is given by

where h and ρ are the effective Hamiltonian and reduced density matrix at layer ℓ (for more details, see ref. [34]). From the singular value decomposition (SVD) of this environment, the updated u is calculated by

$$E_u = USV^\dagger \qquad\qquad u \to -VU^\dagger. \tag{4.14}$$

20

Since this ensures that u is unitary, we are free to symmetrise E_u by

$$E_u \rightarrow E_u + R(E_u) \tag{4.15}$$

before the SVD. This will ensure both unitarity and reflection symmetry. The isometric tensor is symmetrised similarly.

4.2.2 Conformal Data from MERA

Given a MERA representation of a gapless state, it is interesting to see what physical quantities we can compute. The thermodynamic limit of a gapless ground state is described by a conformal field theory (CFT) [31]. Since the isometric tensors perform a rescaling operation, one can compute the eigenvalues of the CFT scaling operator; the scaling dimensions δ_ϕ. These are computed by finding the eigenvalues of the *scaling superoperator*

$$\tag{4.16}$$

The scaling dimensions are then computed via

$$\Delta = \log_3(\lambda). \tag{4.17}$$

One can also compute the central charge of the CFT using eqn. (4.7). Applying this to the effective reduced density matrix on layer L gives accurate estimates of c.
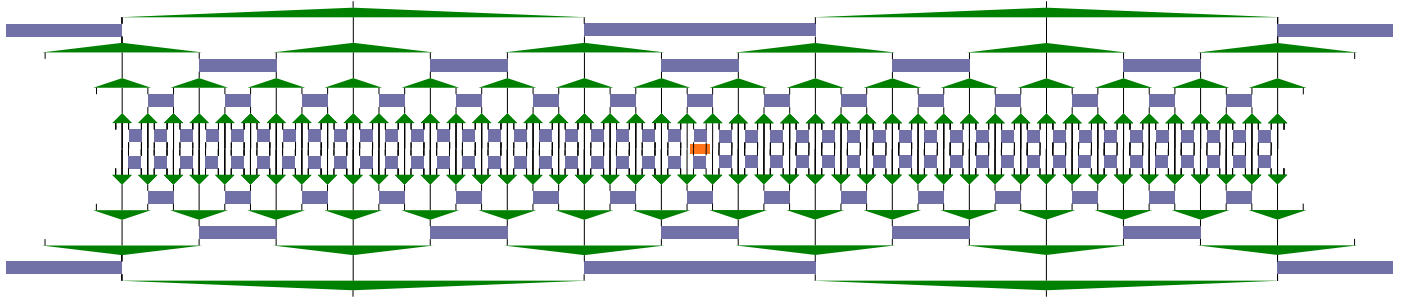
4.2.3 Impurity MERA

In chapter 3, we saw that it is useful to be able to understand the effect of introducing a localised change or impurity in a critical Hamiltonian to the MERA description of the ground state. As one can see from fig. 4.3, when computing the expectation value of a local operator o, only a small number of tensors are required. These are known as the causal cone of the region acted upon by o. This motivates the principle of *minimal update* [40]. This states that if an impurity is introduced into a Hamiltonian in region $\mathcal{R}$, only those tensors in the causal cone of $\mathcal{R}$ require update. There exists much numerical evidence for this assumption [39].

Because each layer of the MERA represents the system on a different length scale, so we see that the impurity has an effect on the system at all distances, not just locally.

If the impurity is scale invariant, we simply need a new pair of tensors $\{u_i, w_i\}$ to describe the causal cone. For convenience, we use a slightly modified ansatz following [39]. The impurity MERA is shown in fig. 4.3c. From this ansatz, conformal data can be computed using the scaling superoperator (eqn. (4.16)) built using the impurity tensors.

In this chapter, we have introduced two numerical methods that can be applied to understand the thermodynamic limit of critical spin chain, both translationally invariant and with an impurity. We have explained how to extract data allowing identification of the conformal field theory describing the thermodynamic limit, including the central charge and the scaling dimensions. These methods can be applied complementarily. For example, we do not know how to compute the conformal spin (related to the momentum in the lattice model) using the MERA, but this is simple to compute using ED. Conversely, the MERA seems to provide robust approximations to the central charge, which may not be obtainable by fitting eqn. (4.7) to the relatively short chains within the realm of ED. Benchmarking results for these techniques are included in appendix A.

(a) Computing the expectation value of a local operator $\langle\psi|o|\psi\rangle$.
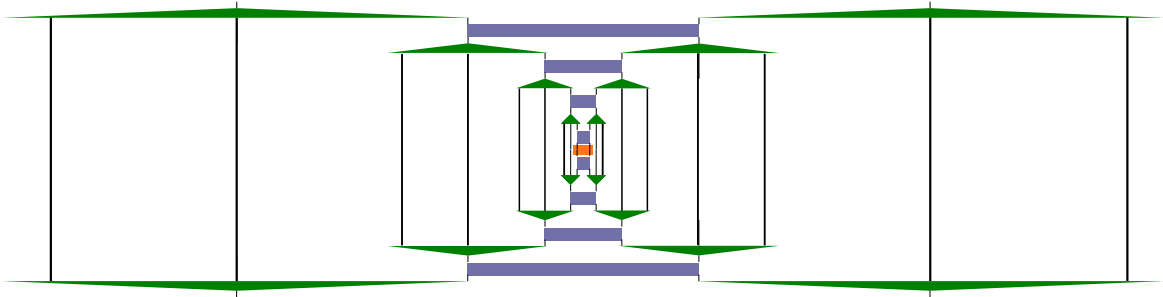
(b) By applying the constraints eqn. (4.8), we see that most of the tensors are not affected.
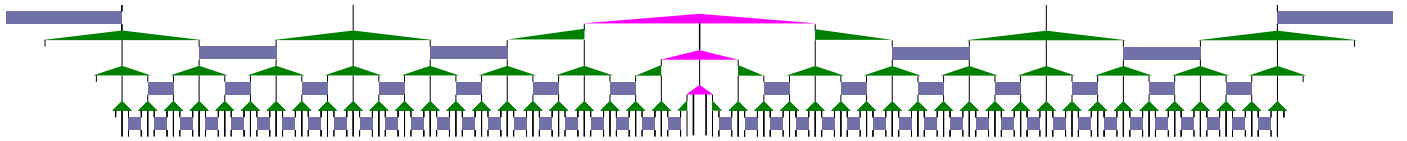
(c) The impurity MERA is obtained by first optimising a bulk MERA (from the Hamiltonian without the defect). The tensors in the causal cone are then updated to capture the effect of the impurity.

Figure 4.3 : Upon the insertion of a local operator, only the tensors in the *causal cone* will be affected. This motivates the principle of minimal update [40]. This allows the impurity MERA to be obtained by updating only the tensors in the causal cone of the defect.

Chapter 5

Conformal Spectra of the Edge Hamiltonians

In chapter 3, we constructed effective Hamiltonians describing the edges of (2+1)-dimensional SPT systems. We built these based on the ansatz given in refs. [1, 2], by assuming a $\mathcal{H}^3(G, U(1))$ phase classification leading to non-onsite edge symmetries associated to 3-cocycles. Since there are three classes of 3-cocycles, there are three classes of Hamiltonian known as Types I, II and III. Type I has been studied in ref. [1]. In this chapter, we will use the techniques described in chapter 4 to investigate the Type II and III models. We will study their properties on both periodic and twisted boundaries, where the twisted boundaries are associated with insertion of a gauge flux. We begin with the Type II model.

5.1 Type II

The Hamiltonian for the Type II model in the nontrivial phase is (eqn. (3.19))

$$H_{II} = -\lambda \sum_{j=1}^{M} (2X_j^{\{1\}} + X_j^{\{2\}} - Z_{j-1}^{\{2\}} X_j^{\{2\}} Z_{j+1}^{\{2\}}), \tag{5.1}$$

where the symmetries are

$$S^{\{1\}} = \prod_{j=1}^{M} X_j^{\{1\}} \prod_{j=1}^{M} \exp\left(-\frac{\pi i}{4}(1 - Z_j^{\{2\}} Z_{j+1}^{\{2\}})\right), \qquad\qquad S^{\{2\}} = \prod_{j=1}^{M} X_j^{\{2\}}. \tag{5.2}$$

Clearly the $\{1\}$-subspace at each site is gapped, with a unique symmetric ground state. By examining the Type I Hamiltonian given in ref. [1], we can identify the Type II Hamiltonian as a gapless model. This is associated to the free boson CFT with compactification radius $R = 2$ [1, 31]. Using the MERA, it is simple to check the spectrum and central charge of the associated CFT to verify this. Our MERA uses bond dimension $\chi = 16$. The numerical central charge is computed to be $c = 1.0065$, agreeing with the above expectation. The observed spectrum is shown in fig. 5.1a, agreeing with the compactification radius $R = 2$.

The primary states can be labelled by a double (n, m), with

$$\Delta = \frac{n^2}{4} + m^2 \tag{5.3}$$

$$(S^{\{1\}}, S^{\{2\}}) = (e^{i\pi m}, e^{i\pi n}), \tag{5.4}$$

where the $\mathbb{Z}_2 \times \mathbb{Z}_2$ charges can be identified from fig. 5.1b. The combined symmetry operation $S^{\{1\}} \times S^{\{2\}}$ has $\mathbb{Z}_2$ charge $e^{i\pi(m+n)}$. Following the arguments in ref. [41], this prevents the gapping of the system since the mass terms will not be symmetry respecting.
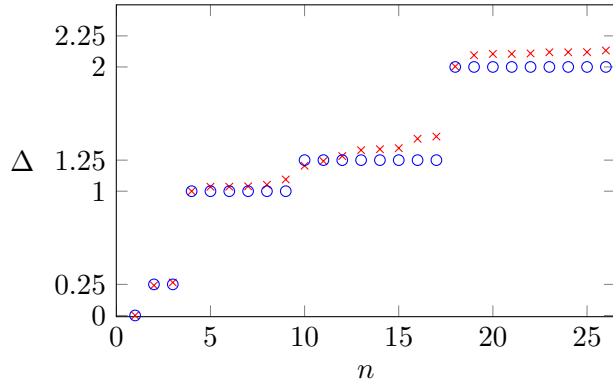
(a) The MERA spectrum of the Type II Hamiltonian obtained from a $\chi = 16$ MERA. The $\times$ are the numerical results, whilst $\circ$ indicate the spectrum expected for the $R = 2$ compactified boson CFT. Reflection symmetry was enforced. The central charge was measured to be $c = 1.0065$.
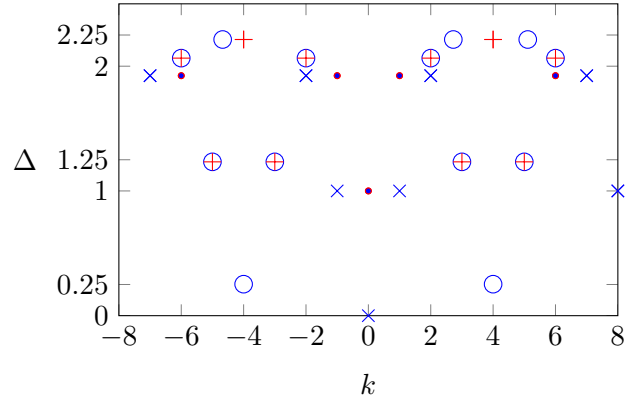
(b) The finite spectrum of the Type II Hamiltonian on 16 sites with the $\{1\}$ subsystem neglected. The spectrum is shifted such that the ground state sits at $\Delta = 0$ and rescaled by $H \rightarrow .64H$ to ensure that descendant fields are separated by 1 unit from their primaries [32]. Under $(S^{\{1\}}, S^{\{2\}})$, the states transform as: $\times = (1, 1)$, $\circ = (1, -1)$, $\bullet = (-1, 1)$ and $+ = (-1, -1)$.

Figure 5.1 : The spectra obtained using MERA and exact diagonalisation of the Type II model on periodic boundaries. Both are consistent with the $R = 2$ compactified free boson being the appropriate CFT for describing the thermodynamic limit. The counting and Δ of states appears to be consistent up to low χ and finite size effects.

5.2 Type III
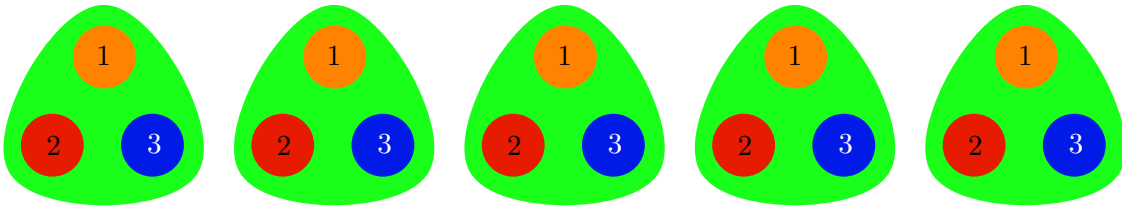
Figure 5.2 : We can think of the Type III Hamiltonian as acting on composite sites with three spin-$1/2$ subsystems. If there are M sites on the chain, we can imagine a chain of length M consisting of only subsystem 1 spins and a chain of length $2M$, with subsystem 2 spins forming the odd numbered sites and subsystem 3 spins forming the even sites.

The Hamiltonian for the Type III model in the nontrivial phase is (eqn. (3.26))

$$H_{III} = -4 \sum_{j=1}^{M} (2X_j^{\{1\}} + X_j^{\{2\}} + X_j^{\{3\}} + Z_{j-1}^{\{3\}} X_j^{\{2\}} Z_j^{\{3\}} + Z_j^{\{2\}} X_j^{\{3\}} Z_{j+1}^{\{2\}}), \tag{5.5}$$

where the symmetries are

$$S^{\{1\}} = \prod_{j=1}^{M} X_j^{\{1\}} \prod_{j=1}^{M} \left[Z_j^{\{2\}} Z_{j+1}^{\{2\}} \right]^{\frac{\log Z_j^{\{3\}}}{i\pi}}, \qquad S^{\{2\}} = \prod_{j=1}^{M} X_j^{\{2\}}, \qquad S^{\{3\}} = \prod_{j=1}^{M} X_j^{\{3\}}. \tag{5.6}$$

Once again the $\{1\}$-subspace at each site is gapped, with a unique symmetric ground state. The $\{2\}, \{3\}$-subspace forms an effective single chain with a Hamiltonian very similar to that in the Type I and II cases up to a relative minus sign between the single and three body terms. Due to this sign change, we can exactly solve the Hamiltonian eqn. (3.26) using a duality transformation onto the XXZ model followed by a Jordan-Wigner transformation.

5.2.1 Exact Solution for Type III Hamiltonian

First, we are going to perform a duality mapping. Let

$$X_j^{\{1\}} \mapsto \bar{X}_j \qquad\qquad X_j^{\{2\}} \mapsto X_{2j-1}X_{2j} \qquad\qquad X_j^{\{3\}} \mapsto Y_{2j-1}Y_{2j} \tag{5.7}$$

$$Z_j^{\{1\}} \mapsto \bar{Z}_j \qquad\qquad Z_j^{\{2\}} \mapsto Y_{2j-1} \qquad\qquad Z_j^{\{3\}} \mapsto X_{2j} \tag{5.8}$$

$$Y_j^{\{1\}} \mapsto \bar{Y}_j \qquad\qquad Y_j^{\{2\}} \mapsto -Z_{2j-1}X_{2j} \qquad\qquad Y_j^{\{3\}} \mapsto Y_{2j-1}Z_{2j}. \tag{5.9}$$

This local unitary mapping brings the above Hamiltonian to

$$H = -4\sum_{j=1}^{M}(2\bar{X}_j + X_{2j-1}X_{2j} + Y_{2j-1}Y_{2j}) - 4\sum_{j=1}^{M-1}(Y_{2j}Y_{2j+1} + X_{2j}X_{2j+1}) - 4(Y_{2M}Y_1 + X_{2M}X_1) \tag{5.10}$$

$$= -8\sum_{j=1}^{M}\bar{X}_j - 4\sum_{j=1}^{2M-1}(Y_jY_{j+1} + X_jX_{j+1}) - 4(Y_{2M}Y_1 + X_{2M}X_1), \tag{5.11}$$

which we recognise as the XX model on a ring of length $2M$ coupled to a product state of length M. We can now use a standard Jordan-Wigner mapping to map this onto a free fermion model. Let

$$\bar{X}_j \mapsto 1 - 2a_j^\dagger a_j \qquad\qquad X_j \mapsto \prod_{k=1}^{j-1}(1 - 2b_k^\dagger b_k)(b_j^\dagger + b_j) \tag{5.12}$$

$$Z_j \mapsto 1 - 2b_j^\dagger b_j \tag{5.13}$$

$$Y_j \mapsto i\prod_{k=1}^{j-1}(1 - 2b_k^\dagger b_k)(b_j^\dagger - b_j). \tag{5.14}$$

These are two species of fermions, with the (anti)-commutation relations

$$\{a_j, a_k\} = \{b_j, b_k\} = 0 \tag{5.15}$$

$$\{a_j, a_k^\dagger\} = \{b_j, b_k^\dagger\} = \delta_{jk} \tag{5.16}$$

$$[a_j, b_k] = [a_j, b_k^\dagger] = 0. \tag{5.17}$$

The Hamiltonian then transforms to

$$H = -8\sum_{j=1}^{M}(1 - 2a_j^\dagger a_j) - 4\sum_{j=1}^{2M-1}((b_j^\dagger - b_j)(b_{j+1}^\dagger + b_{j+1}) - (b_j^\dagger + b_j)(b_{j+1}^\dagger - b_{j+1}))$$

$$-4\prod_{j=1}^{2M}(1-2b_k^\dagger b_k)\left((b_{2M}^\dagger+b_{2M})(b_1^\dagger-b_1)-(b_{2M}^\dagger-b_{2M})(b_1^\dagger+b_1)\right) \tag{5.18}$$

$$=-8\sum_{j=1}^{M}(1-2a_j^\dagger a_j)-8\sum_{j=1}^{2M-1}(b_j^\dagger b_{j+1}+b_{j+1}^\dagger b_j)+8\prod_{j=1}^{2M}(1-2b_k^\dagger b_k)\left(b_{2M}^\dagger b_1+b_1^\dagger b_{2M}\right) \tag{5.19}$$

$$=-8\sum_{j=1}^{M}(1-2a_j^\dagger a_j)-8\sum_{j=1}^{2M-1}(b_j^\dagger b_{j+1}+b_{j+1}^\dagger b_j)-8e^{i\pi(N+1)}\left(b_{2M}^\dagger b_1+b_1^\dagger b_{2M}\right), \tag{5.20}$$

where

$$N=\sum_{j=1}^{2M}b_j^\dagger b_j \tag{5.21}$$

is the total number operator for the chain and we have used the fact that $1-2b_j^\dagger b_j=\exp\left(i\pi b_j^\dagger b_j\right)$. At this point it is convenient to relabel our sites, giving

$$H=-8\sum_{j=0}^{M-1}(1-2a_j^\dagger a_j)-8\left[\sum_{j=0}^{2M-2}(b_j^\dagger b_{j+1}+b_{j+1}^\dagger b_j)+e^{i\pi(N+1)}\left(b_{2M-1}^\dagger b_0+b_0^\dagger b_{2M-1}\right)\right]. \tag{5.22}$$

We would like to diagonalise this, but we have this inconvenient phase term arising from the boundary, which will be $+1$ if there are an odd number of (b-type) fermions in the system, and -1 for an even number. Without the boundary phase, we would do a Fourier transform using

$$b_j=\frac{1}{\sqrt{2M}}\sum_{k=0}^{2M-1}e^{\frac{i\pi jk}{M}}\tilde{b}_k. \tag{5.23}$$

To deal with the boundary term we introduce a site dependant phase into the Fourier transform [42]

$$b_j=\frac{1}{\sqrt{2M}}e^{\frac{i\pi\phi_j}{M}}\sum_{k=0}^{2M-1}e^{\frac{i\pi jk}{M}}\tilde{b}_k. \tag{5.24}$$

We can determine the appropriate phase by insisting that the phases of the $b_j^\dagger b_{j+1}$ ($j<2M-2$) are the same as the phase of the boundary term, so

$$e^{\frac{i\pi(\phi_{j+1}-\phi_j)}{M}}=e^{i2\pi\phi}e^{\frac{i\pi(\phi_{2M-1}-\phi_0)}{M}}, \tag{5.25}$$

where $2\phi=N+1\mod 2$. This can be solved by letting

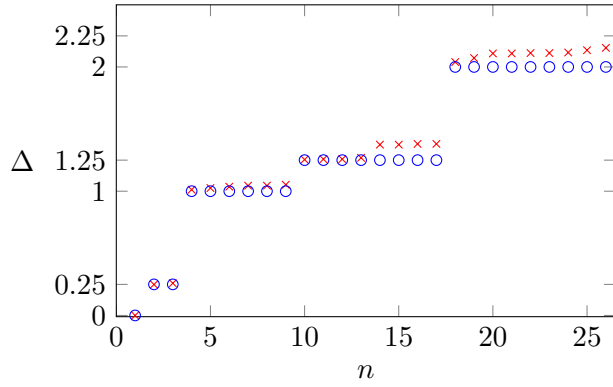$$\phi_j=j(4M-1)\phi\equiv-j\phi. \tag{5.26}$$

The 'twisted' Fourier transform is then
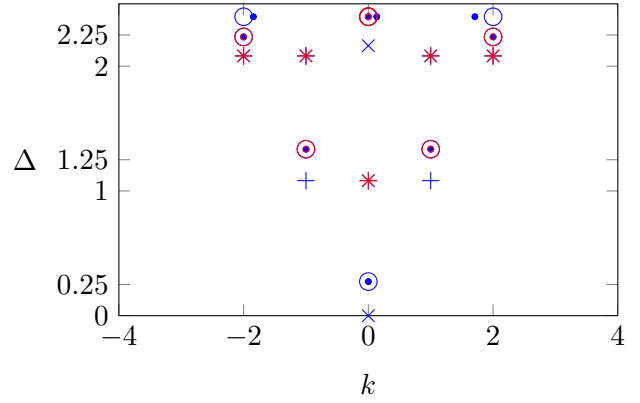
$$b_j=\frac{1}{\sqrt{2M}}\sum_{k=0}^{2M-1}e^{\frac{i\pi j(k-\phi)}{M}}\tilde{b}_k. \tag{5.27}$$

With this,

$$b_{j+1}^\dagger b_j=\frac{1}{2M}\sum_{k,k'=0}^{2M-1}e^{\frac{i\pi}{M}j(k'-k)}e^{\frac{i\pi}{M}(\phi-k)}b_k^\dagger b_{k'} \tag{5.28}$$

26

(a) The MERA spectrum of the Type III Hamiltonian obtained from a $\chi = 16$ MERA. The $\times$ are the numerical results, whilst $\circ$ indicate the spectrum expected for the $R = 2$ compactified boson CFT. Reflection symmetry was enforced. The central charge was measured to be $c = 1.0093$.

(b) The finite spectrum of the Type III Hamiltonian on 8 sites with the $\{1\}$ subsystem neglected. The spectrum is shifted such that the ground state sits at $\Delta = 0$ and rescaled by $H \to .69H$ to ensure that descendant fields are separated by 1 unit from their primaries [32]. Under $(S^{\{1\}}, S^{\{2\}}, S^{\{3\}})$, the states transform as: $\times = (1, 1, 1)$, $\circ = (1, 1, -1)$, $\bullet = (1, -1, 1)$, $+ = (1, -1, -1)$, $\times = (-1, 1, 1)$, $\circ = (-1, 1, -1)$, $\bullet = (-1, -1, 1)$ and $+ = (-1, -1, -1)$.

Figure 5.3 : The spectra obtained using MERA and exact diagonalisation of the Type III model on periodic boundaries. Both are consistent with the $R = 2$ compactified free boson being the appropriate CFT for describing the thermodynamic limit. The counting and Δ of states appears to be consistent up to low χ and finite size effects.

$$b_0^\dagger b_{2M-1} = \frac{1}{2M} \sum_{k,k'=0}^{2M-1} e^{\frac{i\pi}{M}(2M-1)(k'-k)} e^{\frac{i\pi}{M}(\phi-k)} b_k^\dagger b_{k'},$$ (5.29)

so we can write

$$H = -8 \sum_{k=0}^{M-1} (1 - 2a_k^\dagger a_k) - 8 \sum_{k=0}^{2M-1} \Lambda_k b_k^\dagger b_k,$$ (5.30)

where

$$\Lambda_k = 2\cos\left(\frac{\pi}{M}(k - \phi)\right)$$ (5.31)

$$\phi = \begin{cases} 0 & \text{if there are an odd number of fermions} \\ \frac{1}{2} & \text{if there are an even number of fermions} \end{cases}$$ (5.32)

5.2.2 Numerical Results

The numerical results shown in fig. 5.3 confirm that the correct CFT is again the $R = 2$ compactified free boson. Once again, the primary states can be labelled by a double (n, m). This time, it is not clear how to write the action of the individual symmetry operators, however we can identify

$$(S^{\{1\}}, S^{\{2\}} \times S^{\{3\}}) = (e^{i\pi m}, e^{i\pi n}).$$ (5.33)

As before, the combined symmetry operation prevents gapping.

27

5.3 Twisted Boundary Conditions

We have also constructed edge models with twisted boundary conditions. In this section, we present the numerical results we have obtained for these models using ED and impurity MERA.

Recall that we used the twisted translation operator $\tilde{T}$ to construct these models. It is convenient to define the twisted momentum eigenstates with momentum $\tilde{k}$ by
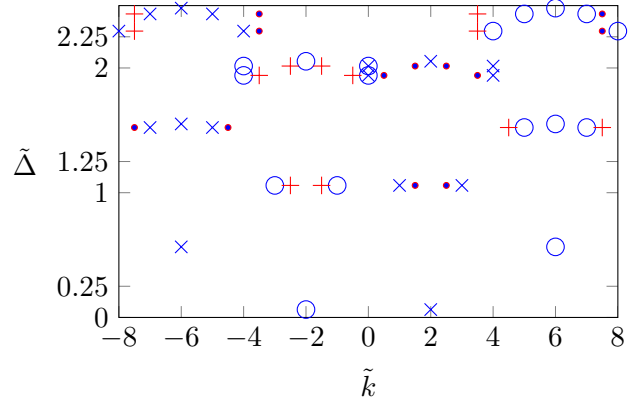
$$\tilde{T}\,|\psi_{\tilde{k}}\rangle = e^{\frac{2\pi i}{M}\tilde{k}}\,|\psi_{\tilde{k}}\rangle. \tag{5.34}$$

Unlike the usual momentum k, this will not be an integer since $\tilde{T}^{2M} = \mathbb{1}$, rather than $T^M = \mathbb{1}$.

5.3.1 Type II
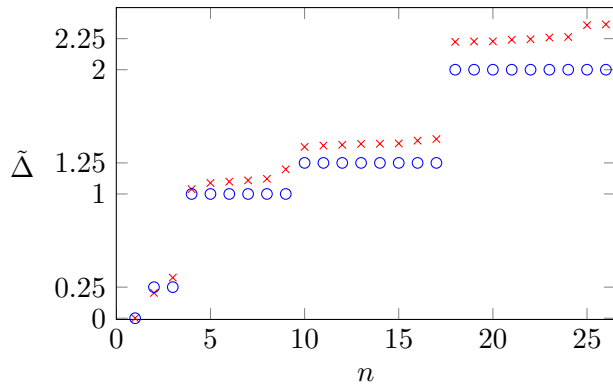
(a) The MERA spectrum of the twisted Type II Hamiltonian obtained from a $\chi = 16$, $\chi_b = 24$ impurity MERA. The $\times$ are the numerical results, whilst $\circ$ indicate the spectrum expected for the $R = 2$ compactified boson CFT with *periodic* boundaries.

(b) The finite spectrum of the twisted Type II Hamiltonian on 16 sites with the $\{1\}$ subsystem neglected. The spectrum is shifted by the same amount as fig. 5.1b and rescaled by $H \to .64H$. Under $(\tilde{S}^{\{1\}}, S^{\{2\}})$, the states transform as: $\times = (1,1)$, $\circ = (1,-1)$, $\bullet = (-1,1)$ and $+ = (-1,-1)$.

Figure 5.4 : The spectra obtained using MERA and exact diagonalisation of the twisted Type II model on periodic boundaries. Clearly these spectra do no agree. The MERA spectrum is essentially identical to that in fig. 5.1a. We do not yet have an explanation for this.

The results obtained for the twisted Type II model (eqn. (3.43)) are shown in fig. 5.4. We do not see agreement between the MERA and ED results, although the MERA results are identical to those obtained for the periodic model. This leads us to doubt the validity of these results, although we do not yet have an explanation for this.

The exact diagonalisation results allow us to identify the scaling dimensions. Again they can be labelled by a pair of integers (n, m), such that

$$\tilde{\Delta} = \frac{1}{4}\left(n + \frac{1}{2}\right)^2 + m^2, \tag{5.35}$$

$$(\tilde{S}^{\{1\}}, S^{\{2\}}) = (e^{i\pi m}, e^{i\pi n}). \tag{5.36}$$

This differs from the Type I case, were we expect to see

$$\tilde{\Delta} = \frac{1}{4}\left(n + \frac{1}{2}\right)^2 + \left(m + \frac{1}{2}\right)^2. \tag{5.37}$$

This seems to be due to the choice of $\mathbb{Z}_2$ flux inserted. We twist with respect to the first symmetry only. In contrast to the Type I case, the string of X_j operators commutes with the Hamiltonian vanishes, with only the non-onsite part of the symmetry contributing to the symmetry. In the CFT, this seems to be linked to only one of the charges changing [2].

5.3.2 Type III
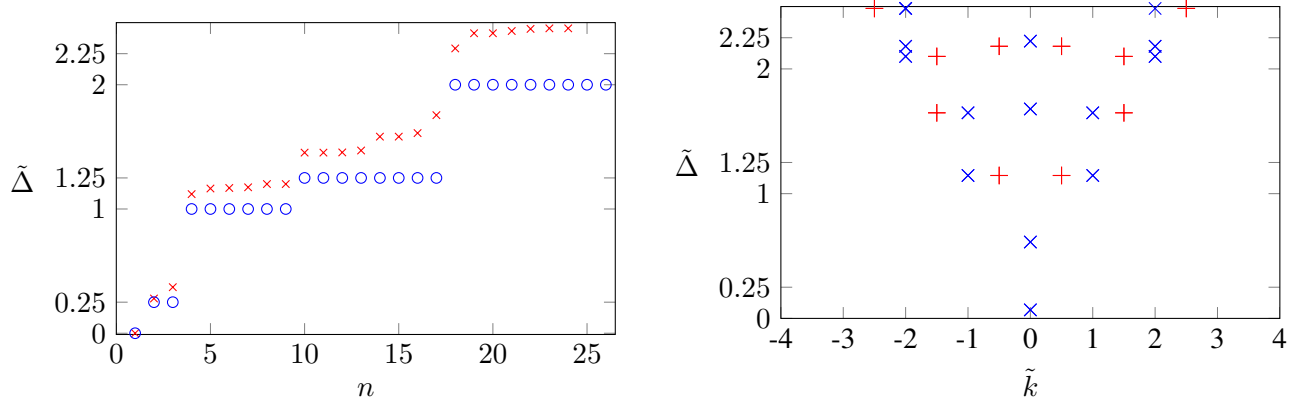
(a) The MERA spectrum of the twisted Type III Hamiltonian obtained from a $\chi = 16$, $\chi_b = 24$ impurity MERA. The $\times$ are the numerical results, whilst $\circ$ indicate the spectrum expected for the $R = 2$ compactified boson CFT *periodic* boundaries.

(b) The finite spectrum of the twisted Type III Hamiltonian on 8 sites with the $\{1\}$ subsystem neglected. The spectrum is shifted by the same amount as fig. 5.3b and rescaled by $H \to .69H$. Under $(\tilde{S}^{\{1\}})$, the states transform as: $\times = 1$ and $+ = -1$. Note that all states are doubly degenerate.

Figure 5.5 : The spectra obtained using MERA and exact diagonalisation of the twisted Type III model on periodic boundaries. Clearly these spectra do no agree. We do not yet have an explanation for this.

The results obtained for the twisted Type III model (eqn. (3.49)) are shown in fig. 5.5. We do not see agreement between the MERA and ED results. Since the MERA seems to have failed in the Type II case, we suspect that the same error is at play here. The exact diagonalisation results allow us to identify the scaling dimensions. Again they can be labelled by a pair of integers (n, m), such that

$$\tilde{\Delta} = \frac{1}{4}\left(n + \frac{1}{2}\right)^2 + m^2. \tag{5.38}$$

In this chapter, we have numerically investigated the models for the gapless edges of (2+1)-dimensional SPT states in their nontrivial phase. We have seen that all three types of Hamiltonian corresponding to the three classes of 3-cocycles are consistent with a $c = 1$ CFT description in the thermodynamic limit. We have seen how enforcing the non-onsite symmetry prevents us from adding a mass term and so gapping out the model. We have obtained spectra for the models on twisted boundary conditions, corresponding to the insertion of a gauge flux. We have seen that this causes a spectral shift, although more analysis is required.

29

Chapter 6

Conclusions and Future Work

In this essay, we have constructed lattice models describing the gapless edges of (2+1)-dimensional symmetry protected topological systems under a finite Abelian group. We have introduced two numerical methods which can be used to study these gapless spin models on both periodic and twisted boundary conditions.

In the fifth chapter, we employed these numerical methods to investigate the edge Hamiltonians constructed. This allowed us to confirm the CFT associated with their thermodynamic limit by obtaining the central charge and conformal spectra.

The application of the impurity MERA to the twisted Hamiltonians has failed to recover the expected results (including for the Ising model in appendix A). If the results do not improve upon increasing the bond dimension, other culprits should be investigated. The onsite symmetry of the models can be enforced in the MERA. Due to the complex nature of the algorithm, it is unclear whether this would help, but enforcing symmetries has proven fruitful in the past [39]. Another avenue is to investigate the assumption of conformal invariance of the defect which has gone into our impurity MERA algorithm.

Concerning the MERA, it would be interesting to investigate how MPO or non-onsite symmetries could be enforced in the tensor network. Presumably this would both speed up the algorithm and ensure that the final state is symmetry respecting.

We have not analysed the spectra obtained for the models when they are placed on twisted boundary conditions. These give experimental access to the group cohomology labels, since the spectra are expected to shift in ways which differ in each phase [43]. Understanding these spectra is an obvious next step.

References

[1] L. H. Santos and J. Wang, "Symmetry-protected many-body Aharonov-Bohm effect", Phys. Rev. B **89**, 195122, `arXiv:1310.8291` (2014).

[2] J. Wang, L. H. Santos, and X.-G. Wen, "Bosonic Anomaly, Induced Fractional Quantum Number and Degenerate Zero Modes - the anomalous edge physics of Symmetry Protected Topological States" , `arXiv:1403.5256` (2014).

[3] L. D. Landau and E. Lifshitz, *Statistical Physics, Volume 5* (Elsevier, 1996).

[4] L. van Hove, "Sur L'intégrale de Configuration Pour Les Systèmes De Particules À Une Dimension", Physica **16**, 137 (1950).

[5] S. Sachdev, *Quantum Phase Transitions* (Cambridge University Press, 2001).

[6] N. D. Mermin and H. Wagner, "Absence of Ferromagnetism or Antiferromagnetism in One- or Two-Dimensional Isotropic Heisenberg Models", Phys. Rev. Lett. **17**, 1133 (1966).

[7] H. Stanley, "Dependence of Critical Properties on Dimensionality of Spins", Phys. Rev. Lett. **20**, 589 (1968).

[8] J. M. Kosterlitz and D. J. Thouless, "Ordering, metastability and phase transitions in two-dimensional systems", J. Phys. C **6**, 1181 (1973).

[9] X. Chen, Z.-C. Gu, and X.-G. Wen, "Local unitary transformation, long-range quantum entanglement, wave function renormalization, and topological order", Phys. Rev. B **82**, 155138 (2010).

[10] X. Chen, Z.-X. Liu, and X.-G. Wen, "2D symmetry protected topological orders and their protected gapless edge excitations", Phys. Rev. B **84**, 235141, `arXiv:1106.4752` (2011).

[11] X.-G. Wen, "Topological Order: From Long-Range Entangled Quantum Matter to a Unified Origin of Light and Electrons", ISRN Condens. Matter Phys. **2013**, `arXiv:1210.1281` (2013).

[12] H. Bombin, in *Quantum Error Correction*, edited by D. Lidar and T. Brun (Cambridge University Press, New York, 2013), `arXiv:1311.0277`.

[13] E. Dennis, A. Kitaev, A. Landahl, and J. Preskill, "Topological quantum memory", J. Math. Phys. **43**, 4452, `arXiv:quant-ph/0110143` (2002).

[14] C. Nayak, A. Stern, M. Freedman, and S. Das Sarma, "Non-Abelian anyons and topological quantum computation", Rev. Mod. Phys. **80**, 1083, `arXiv:0707.1889` (2008).

[15] G. K. Brennen and J. K. Pachos, "Why should anyone care about computing with anyons?", Proc. R. Soc. A **464** (2008).

[16] J. E. Moore, "The birth of topological insulators.", Nature **464**, 194 (2010).

[17] F. Verstraete and J. Cirac, "Matrix product states represent ground states faithfully", Phys. Rev. B **73**, 094423 (2006).

[18] M. B. Hastings, "An area law for one-dimensional quantum systems", J. Stat. Mech. Theor. Exp. **2007**, P08024 (2007).

[19] N. Schuch, D. Pérez-García, and I. Cirac, "Classifying quantum phases using matrix product states and projected entangled pair states", Phys. Rev. B **84**, 165139, `arXiv:1010.3732` (2011).

[20] M. Hastings, "Entropy and entanglement in quantum ground states", Phys. Rev. B **76**, 035114, `arXiv:cond-mat/0701055` (2007).

[21] F. Verstraete, V. Murg, and J. Cirac, "Matrix product states, projected entangled pair states, and variational renormalization group methods for quantum spin systems", Adv. Phys. **57**, 143, `arXiv:0907.2796` (2008).

[22] M. de Wild Propitius, "(Spontaneously broken) Abelian Chern-Simons theories", Nucl. Phys. B **489**, 297, `arXiv:hep-th/9606029` (1997).

[23] Y.-Y. Shi, L.-M. Duan, and G. Vidal, "Classical simulation of quantum many-body systems with a tree tensor network", Phys. Rev. A **74**, 022320, `arXiv:quant-ph/0511070` (2006).

[24] K. L. Brown, W. J. Munro, and V. M. Kendon, "Using Quantum Computers for Quantum Simulation", Entropy **12**, 2268, `arXiv:1004.5528` (2010).

[25] F. Verstraete and J. I. Cirac, "Continuous Matrix Product States for Quantum Fields", Phys. Rev. Lett. **104**, 190405 (2010).

[26] J. Haegeman, T. J. Osborne, and F. Verstraete, "Post-matrix product state methods: To tangent space and beyond", Phys. Rev. B **88**, 075133, `arXiv:1305.1894` (2013).

[27] E. Stoudenmire and S. R. White, "Studying Two-Dimensional Systems with the Density Matrix Renormalization Group", Annu. Rev. Condens. Matter Phys. **3**, 111, `arXiv:1105.1374` (2012).

[28] K. H. Marti and M. Reiher, "The Density Matrix Renormalization Group Algorithm in Quantum Chemistry", Z. Phys. Chem. **224**, 583 (2010).

[29] G. Vidal, "Efficient Classical Simulation of Slightly Entangled Quantum Computations", Phys. Rev. Lett. **91**, 147902, `arXiv:quant-ph/0301063` (2003).

[30] G. Vidal, "13/14 PSI - Explorations in Condensed Matter - Lecture 4", URL `http://pirsa.org/14040025`.

[31] P. Di Francesco, *Conformal field theory* (Springer, New York, 1997).

[32] P. Christe and M. Henkel, *Conformal Invariance and Critical Phenomena* (Springer, Berlin; Heidelberg, 1993).

[33] G. Vidal, "Entanglement Renormalization", Phys. Rev. Lett. **99**, 220405 (2007).

[34] G. Evenbly and G. Vidal, "Algorithms for entanglement renormalization", Phys. Rev. B **79**, 144108 (2009).

[35] R. Pfeifer, G. Evenbly, and G. Vidal, "Entanglement renormalization, scale invariance, and quantum criticality", Phys. Rev. A **79**, 040301 (2009).

[36] G. Vidal, J. I. Latorre, E. Rico, and A. Kitaev, "Entanglement in Quantum Critical Phenomena", Phys. Rev. Lett. **90**, 227904 (2003).

[37] J. Eisert, "Colloquium: Area laws for the entanglement entropy", Rev. Mod. Phys. **82**, 277 (2010).

[38] H.-W. Chang, Y.-D. Hsieh, and Y.-J. Kao, "Detection of symmetry-protected topological phases in one dimension with multiscale entanglement renormalization" , `arXiv:1305.2663` (2013).

[39] G. Evenbly and G. Vidal, "Algorithms for entanglement renormalization: boundaries, impurities and interfaces" , `arXiv:1312.0303` (2013).

[40] G. Evenbly and G. Vidal, "A theory of minimal updates in holography" , arXiv:1307.0831 (2013).

[41] X. Chen and X.-G. Wen, "Chiral symmetry on the edge of two-dimensional symmetry protected topological phases", Phys. Rev. B **86**, 235135, arXiv:1206.3117 (2012).

[42] A. De Pasquale, G. Costantini, P. Facchi, G. Florio, S. Pascazio, and K. Yuasa, "XX model on the circle", Eur. Phys. J. Spec. Top. **160**, 127 (2008).

[43] X.-G. Wen, "Symmetry-protected topological invariants of symmetry-protected topological phases of interacting bosons and fermions", Phys. Rev. B **89**, 035147, arXiv:1301.7675 (2014).

[44] M. Oshikawa and I. Affleck, "Boundary conformal field theory approach to the critical two-dimensional Ising model with a defect line", Nucl. Phys. B **495**, 533, arXiv:cond-mat/9612187 (1997).

[45] X. Chen, Z.-C. Gu, Z.-X. Liu, and X.-G. Wen, "Symmetry protected topological orders and the group cohomology of their symmetry group", Phys. Rev. B **87**, 155114, arXiv:1106.4772 (2013).

Appendix A

Benchmarking The Code

In chapter 4, we introduced a complementary pair of numerical methods which can be utilised to investigate the properties of gapless lattice models. The exact diagonalisation (ED) algorithm allows for extraction of the conformal spectrum, including the symmetry of the states. Accessing data related to the central charge can in principle be computed, however this requires scaling of the ground state and a fit. Given the system sizes accessible, this fit can be tricky and inaccurate. The Multiscale Entanglement Renormalisation Ansatz (MERA) on the other hand, allows for simple, accurate calculation of the central charge and conformal spectrum (directly in the thermodynamic limit), however it is not known how to identify the symmetry of the operators under the non-onsite symmetry present in our models.

In this appendix, we demonstrate the capabilities of our implementations.

A.1 Ising Model with an Impurity

As a demonstration, we will use the Ising model with an impurity to test both the ED and impurity MERA implementations. This is described by

$$
H = -\sum_{j=1}^{M} X_j - \sum_{j=1}^{M-1} Z_j Z_{j+1} - \alpha Z_M Z_1, \tag{A.1}
$$

where α describes the strength of the interaction between sites M and 1. If $\alpha = 1$, we have the usual Ising model. If $\alpha = 0$, there is no coupling. The antiperiodic boundary conditions discussed in chapter 3 correspond to $\alpha = -1$. The symmetry of this model is $\mathbb{Z}_2$, realised by
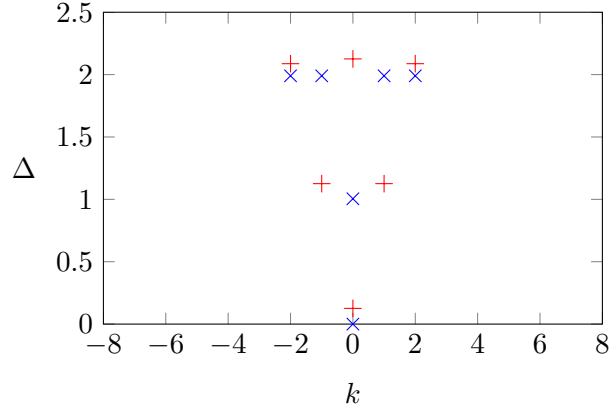
$$
S^{\{1\}} = \prod_{j=1}^{M} X_j \tag{A.2}
$$

for all values of the coupling parameter.

At the pure Ising point ($\alpha = 0$), we can apply three techniques; exact diagonalisation, standard (bulk) MERA, and impurity MERA where the impurity Hamiltonian is taken to be the same as the rest of the chain. Note that the form of the MERA is still changed, we use the altered form shown in fig. 4.3c and reoptimise the impurity tensors. The results for an ED and $\chi = 14$ MERA/impurity MERA are shown in fig. A.1. These replicate the values expected from the free fermion CFT which is known to describe the Ising model in the thermodynamic limit.

For $\alpha \neq 1$, the spectrum has been obtained analytically using boundary conformal field theory [44], and using impurity MERA [39]. The scaling dimensions are expected to be
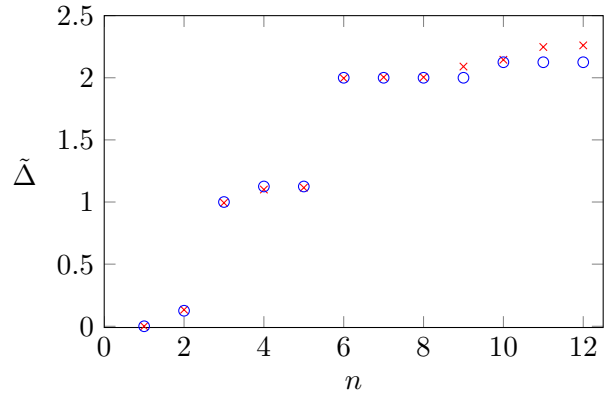
$$
\tilde{\Delta}(\alpha) = 2\left(m + \frac{1}{4} + \frac{\theta(\alpha)}{\pi}\right)^2, \qquad\qquad \theta(\alpha) + \tan^{-1}\left(\frac{1-\alpha}{1+\alpha}\right) \tag{A.3}
$$

(a) The ED spectrum for the pure Ising model on 16 sites. Under S, the states transform as: $\times = 1$ and $+ = -1$.
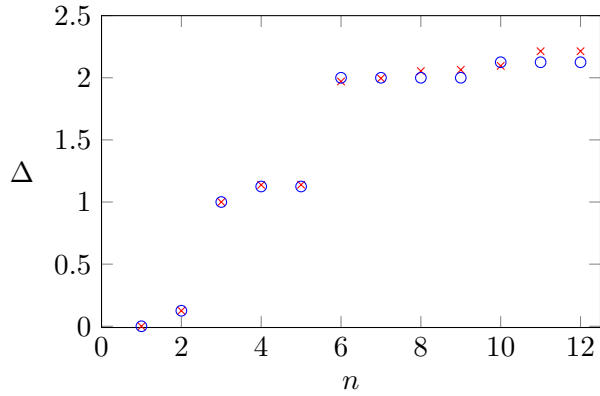
(b) The bulk MERA spectrum of the pure Ising model with $\chi = 14$. The $\times$ are the numerical results, whilst $\circ$ indicate the spectrum expected for the free fermion CFT. Reflection symmetry was enforced.

(c) The impurity MERA spectrum of the pure Ising model with $\chi = 14$, $\chi_b = 21$. The $\times$ are the numerical results, whilst $\circ$ indicate the spectrum expected for the free fermion CFT. Reflection symmetry was enforced.

Figure A.1 : The spectra obtained from the pure Ising model (no impurity). (a) was obtained using ED. (b) is the result of a bulk MERA computation whilst (c) used the impurity MERA where the impurity Hamiltonian was identical to the rest of the chain. As expected, all match the free fermion CFT.

Figure A.2 : The impurity MERA spectrum of the Ising model with a defect of strength α. This used $\chi = 14$. The $\times$ are the numerical results, whilst $-$ indicate the spectrum expected for the free fermion CFT with an impurity. Reflection symmetry was enforced.

in the -1 symmetry sector, and retain their bulk values in the $+1$ sector [39]. In fig. A.2, we show the values obtained from a $\chi = 14$, $\chi_b = 21$ impurity MERA for various values of α. We observe accurate recovery of the values expected from eqn. (A.3) for all relevant operators ($\tilde{\Delta} \leq 2$) for all values of α.

We now turn to the antiperiodic (twisted) model ($\alpha = -1$). Applying exact diagonalisation, we recover the scaling dimensions expected for the nonlocal fields in the free fermion CFT [31], as shown in fig. A.3b. The impurity MERA spectrum is shown in fig. A.3a, compared to the *local* scaling dimensions. These are not expected to match, but here we see an unambiguous recovery of these values. Understanding why this is occurring requires more investigation. Due to the accuracy of the results, it seems unlikely that it is due to low bond dimension. It is possible that enforcing the symmetry of the model on the tensors would produce an improvement. The twisting can be though of as applying a half infinite string of the onsite symmetry operator, so if we knew how the tensors transformed under the symmetry we could compute the twisted spectrum directly. This has been achieved previously for a variety of models [34]. It is unclear how this would generalise to the models discussed in chapter 3 due to the non-onsite nature of those symmetries. In this appendix, we have

demonstrated the functionality of our numerical techniques. We have shown accurate recovery of the shift in the spectrum of an impurity model when the impurity corresponds to an altered interaction strength. We have identified a problem with applying the impurity MERA to understand twisted boundary conditions and proposed several solutions.
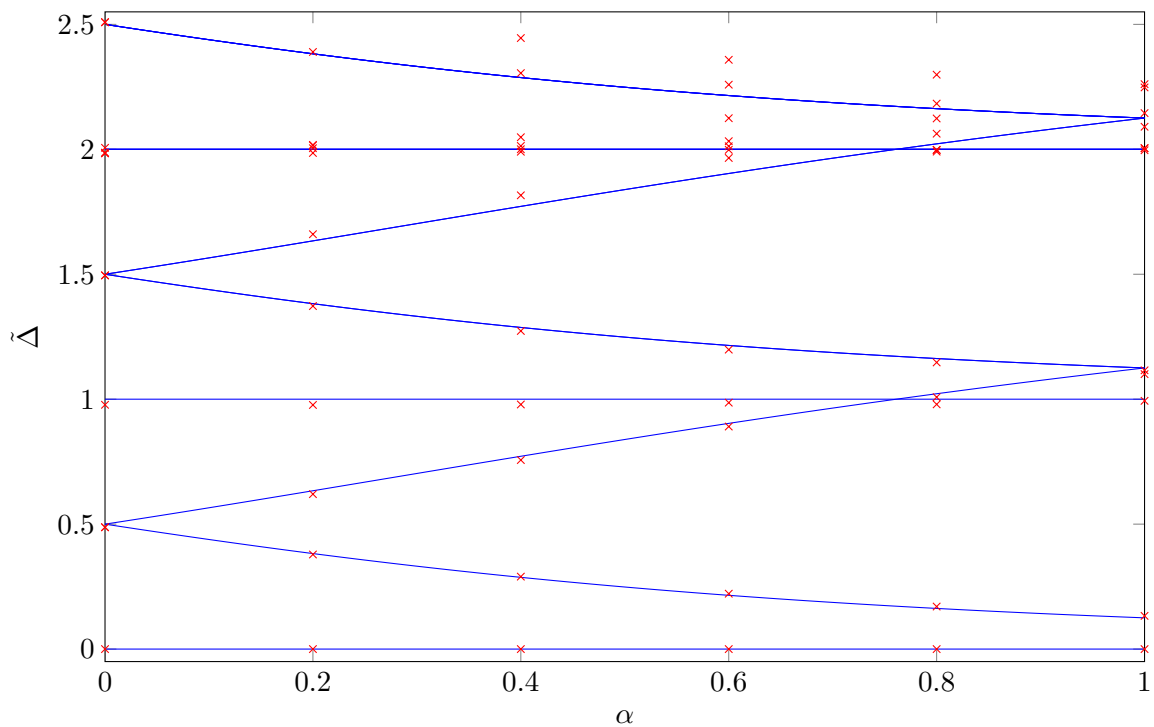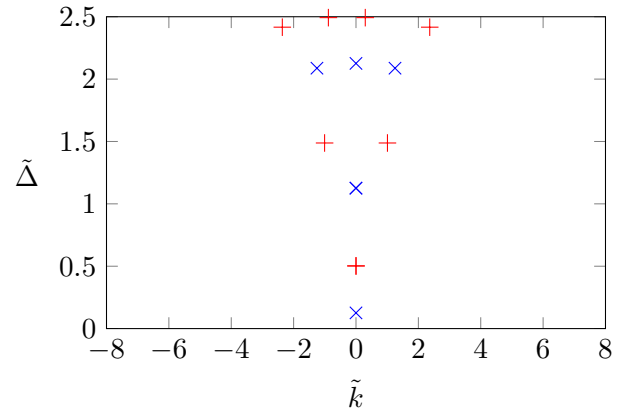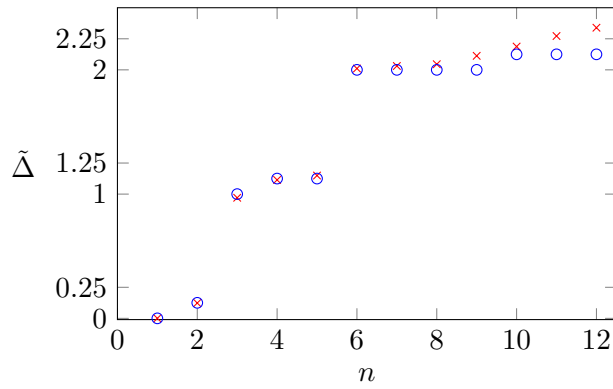
(a) The bulk MERA spectrum of the pure Ising model with $\chi = 14$. The $\times$ are the numerical results, whilst $\circ$ indicate the spectrum expected for the *local* operators in the free fermion CFT. These values are not expected to match. Reflection symmetry was enforced.

(b) The ED spectrum for the twisted ($\alpha = -1$) Ising model on 16 sites. Under S, the states transform as: $\times = 1$ and $+ = -1$.

Figure A.3 : The spectra obtained from the twisted ($\alpha = -1$) Ising model. (a) was obtained using impurity MERA whilst (b) used ED. The ED recovers the nonlocal operators of the free fermion CFT as expected, but the impurity MERA still recovers the local operators. We do not know why this occurs.

Appendix B

More Detailed Lattice Constructions

In this appendix, we provide a more detailed account of the construction of the edge Hamiltonians.

B.1   Type I

We begin the construction by defining a lattice model for the edge of an SPT state protected by a $\mathbb{Z}_N$ symmetry. In the bulk, the symmetry is realised in an onsite manner

$$S_{\text{bulk}} = \prod_{j \in \text{sites}} U_j(g). \tag{B.1}$$

The effective symmetry of the boundary theory will not be onsite however (something about how the protection can be renormalised away).

Following ref. [1], we make the following ansatz for the effective edge $\mathbb{Z}_N$ symmetry operator

$$S_N^{(p)} = \prod_{j=1}^{M} \tau_j \prod_{j=1}^{M} U_{j,j+1}^{(p)}, \tag{B.2}$$

where

$$\tau^N = \sigma^N = \mathbb{1}, \tag{B.3}$$

$$\sigma_j \tau_k = \omega^{\delta_{jk}} \tau_k \sigma_j, \tag{B.4}$$

$$\omega = \exp\left(\frac{2\pi i}{N}\right), \tag{B.5}$$

$$U_{j,j+1}^{(p)} = \exp\left(-\frac{2\pi i}{N^2} p \left\{ \frac{N-1}{2} + \sum_{a=1}^{N-1} \frac{(\sigma_j^\dagger \sigma_{j+1})^a}{\omega^a - 1} \right\}\right), \tag{B.6}$$

and p labels the bulk SPT phase according to the cohomology classification [45]. More concretely, we can choose a basis in which the operators are represented by

$$\sigma = \begin{pmatrix} 1 & 0 & 0 & \cdots & 0 \\ 0 & \omega_a & 0 & \cdots & 0 \\ 0 & 0 & \omega_a^2 & \cdots & 0 \\ 0 & 0 & 0 & \ddots & 0 \\ 0 & 0 & 0 & \cdots & \omega_a^{N_a-1} \end{pmatrix}, \qquad \tau = \begin{pmatrix} 0 & 0 & 0 & \cdots & 0 & 1 \\ 1 & 0 & 0 & \cdots & 0 & 0 \\ 0 & 1 & 0 & \cdots & 0 & 0 \\ 0 & 0 & 1 & \ddots & 0 & 0 \\ 0 & 0 & 0 & \cdots & 1 & 0 \end{pmatrix}. \tag{B.7}$$

For $\mathbb{Z}_2$, this recovers the Pauli operators

$$\sigma = Z = \begin{pmatrix} 1 & 0 \\ 0 & -1 \end{pmatrix}, \qquad\qquad \tau = X = \begin{pmatrix} 0 & 1 \\ 1 & 0 \end{pmatrix}, \tag{B.8}$$

whilst for $\mathbb{Z}_3$, we have

$$\sigma = \begin{pmatrix} 1 & 0 & 0 \\ 0 & e^{2\pi i/3} & 0 \\ 0 & 0 & e^{-2\pi i/3} \end{pmatrix}, \qquad\qquad \tau = \begin{pmatrix} 0 & 0 & 1 \\ 1 & 0 & 0 \\ 0 & 1 & 0 \end{pmatrix}. \tag{B.9}$$

From this symmetry operator, a (translationally invariant) Hamiltonian can be constructed using the ansatz

$$H_N^{(p)} = \sum_{j=1}^{M} \sum_{a=0}^{N-1} S_N^{-a} \tau_j S_N^{a} + hc. \tag{B.10}$$

B.1.1 $\mathbb{Z}_2$ Symmetry

B.1.1.1 Translationally Invariant and Periodic

The construction in the case of a $\mathbb{Z}_2$ symmetry has been explicitly computed in ref. [1], we repeat it here for completeness. In this case, $\omega = -1$, $\sigma = Z$, $\tau = X$. With this, the Hamiltonian becomes

$$H_2^{(p)} = -\lambda \sum_{j=1}^{M} \sum_{a=0}^{N-1} \left(S_N^{(p)}\right)^{-a} X_j \left(S_N^{(p)}\right)^{a} \tag{B.11}$$

$$= -\lambda \sum_{j=1}^{M} X_j + \left(\prod_k U_{k,k+1}^{(p)}{}^{-1}\right)\left(\prod_k X_k^{-1}\right) X_j \left(\prod_k X_k\right)\left(\prod_k U_{k,k+1}^{(p)}\right) \tag{B.12}$$

$$= -\lambda \sum_{j=1}^{M} X_j + \left(U_{j-1,j}^{(p)}{}^{-1} U_{j,j+1}^{(p)}{}^{-1}\right) X_j \left(U_{j-1,j}^{(p)} U_{j,j+1}^{(p)}\right) \tag{B.13}$$

$$= -\lambda \sum_{j=1}^{M} X_j + \left(e^{-\frac{\pi i}{4}p Z_{j-1} Z_j} e^{-\frac{\pi i}{4} p Z_j Z_{j+1}}\right) X_j \left(e^{\frac{\pi i}{4}p Z_{j-1} Z_j} e^{\frac{\pi i}{4} p Z_j Z_{j+1}}\right) \tag{B.14}$$

$$= -\lambda \sum_{j=1}^{M} X_j + \left(e^{-\frac{\pi i}{2}p Z_{j-1} Z_j} e^{-\frac{\pi i}{2} p Z_j Z_{j+1}}\right) X_j. \tag{B.15}$$

Now, we can use the following to evaluate the exponentials

Exponentiating a $\mathbb{Z}_N$ variable
Let σ be some $\mathbb{Z}_N$ variable. Then $$\exp(z\sigma) = \sum_{a=0}^{N-1} A_a(z,N)\sigma^a, \tag{B.16}$$ where $$A_a(z,N) = \sum_{j=0}^{\infty} \frac{z^{a+Nj}}{(a+Nj)!} \tag{B.17}$$

Then the Hamiltonian is

$$H_2^{(p)} = -\lambda \sum_{j=1}^{M} X_j + (-1)^p (Z_{j-1} Z_{j+1})^p X_j, \tag{B.18}$$

or

$$H_2^{(0)} = -\lambda' \sum_{j=1}^{M} X_j, \tag{B.19}$$

$$H_2^{(1)} = -\lambda \sum_{j=1}^{M} (X_j - Z_{j-1} X_j Z_{j+1}). \tag{B.20}$$

B.1.1.2 Twisted Boundary Conditions

It is also of interest to insert a unit of $\mathbb{Z}_N$ flux through the ring. To this end, we repeat the construction from ref. [1]. With a unit of flux, we do not expect the Hamiltonian to be translationally invariant ($[H, T] = 0$), we instead define the *twisted translation operator* $\tilde{T}$ by

$$\tilde{T}^{(p)} = T\, U_{M,1}^{(p)} \tau_1. \tag{B.21}$$

This incorporates the effect of the gauge flux, so we expect the Hamiltonian to be invariant under the application of $\tilde{T}$. Taking the Mth power of $\tilde{T}$, we obtain the *twisted symmetry operator*

$$\tilde{S}_N^{(p)} = \left(\tilde{T}^{(p)}\right)^M \tag{B.22}$$

$$= T\, U_{M,1}^{(p)} \tau_1 T\, U_{M,1}^{(p)} \tau_1 \ldots T\, U_{M,1}^{(p)} \tau_1 T\, U_{M,1}^{(p)} \tau_1 \tag{B.23}$$

$$= T^M\, U_{M-1,M}^{(p)} \tau_M\, U_{M-2,M-1}^{(p)} \tau_{M-1} \ldots U_{1,2}^{(p)} \tau_2\, U_{M,1}^{(p)} \tau_1 \tag{B.24}$$

$$= \mathbb{1}\, U_{M-1,M}^{(p)}\, U_{M-2,M-1}^{(p)} \ldots U_{1,2}^{(p)}\, \tau_M U_{M,1}^{(p)} \tau_{M-1} \ldots \tau_2 \tau_1 \tag{B.25}$$

$$= \prod_{j=1}^{N} U_{j,j+1}^{(p)} \left(U_{M,1}^{(p)}\right)^{-1} \tau_M U_{M,1}^{(p)} \tau_M^\dagger \prod_{k=1}^{N} \tau_k \tag{B.26}$$

$$= \exp\left(\frac{2\pi i}{N^2} p \left\{ \sum_{a=1}^{N-1} \frac{(\sigma_M^\dagger \sigma_1)^a}{\omega^a - 1} - \sum_{b=1}^{N-1} \frac{(\omega \sigma_M^\dagger \sigma_1)^b}{\omega^b - 1} \right\}\right) S_N^{(p)}. \tag{B.27}$$

In the case of $\mathbb{Z}_2$, this becomes

$$\tilde{S}_2^{(0)} = S_2^{(0)} \tag{B.28}$$

$$\tilde{S}_2^{(1)} = \exp\left(-\frac{\pi i}{2} Z_M Z_1\right) S_2^{(1)} \tag{B.29}$$

$$= -i Z_M Z_1 S_2^{(1)}. \tag{B.30}$$

Now, using the result eqns. (B.19) and (B.20), we can construct a Hamiltonian which commutes with $\tilde{T}$. Writing

$$H_2^{(p)} = -\sum_{j=1}^{M} h_j^{(p)}, \tag{B.31}$$

it is clear that most terms will commute with $\tilde{T}$ by construction. The only remaining terms are $h_M^{(1)}$ and $h_1^{(1)}$. We can define

$$
\tilde{h}_j^{(p)} = \begin{cases} h_j^{(p)} & \text{if } j = 2 \ldots M-1 \\ \tilde{T}^\dagger h_{M-1}^{(p)} \tilde{T} & \text{if } j = M \\ \left(\tilde{T}^\dagger\right)^2 h_{M-1}^{(p)} \left(\tilde{T}\right)^2 & \text{if } j = 1. \end{cases}
\tag{B.32}
$$

Given this, we get $\tilde{H}_2^{(0)} = H_2^{(0)}$, and

$$
\tilde{h}_M^{(1)} = \tau_1^\dagger \left(U_{M,1}^{(1)}\right)^{-1} T^\dagger (X_{M-1} - Z_{M-2}X_{M-1}Z_M) T U_{M,1}^{(1)} \tau_1
\tag{B.33}
$$

$$
= X_1 \exp\left(-\frac{\pi i}{4} Z_M Z_1\right) (X_M - Z_{M-1}X_M Z_1) \exp\left(\frac{\pi i}{4} Z_M Z_1\right) X_1
\tag{B.34}
$$

$$
= i Z_M Z_1 (X_M + Z_{M-1}X_M Z_1)
\tag{B.35}
$$

$$
= -Y_M Z_1 - Z_{M-1} Y_M
\tag{B.36}
$$

$$
\tilde{h}_1^{(1)} = i X_1 \exp\left(-\frac{\pi i}{4} Z_M Z_1\right) (Z_1 X_1 Z_2 + Z_M Z_1 X_1) \exp\left(\frac{\pi i}{4} Z_M Z_1\right) X_1
\tag{B.37}
$$

$$
= -i \exp\left(\frac{\pi i}{2} Z_M Z_1\right) (Z_1 X_1 Z_2 + Z_M Z_1 X_1)
\tag{B.38}
$$

$$
= Z_M X_1 Z_2 + X_1.
\tag{B.39}
$$

For consistency, we check that $\tilde{T}^\dagger \tilde{h}_1^{(1)} \tilde{T} = h_2^{(1)}$:

$$
\tilde{T}^\dagger \tilde{h}_1^{(1)} \tilde{T} = X_1^\dagger \left(U_{M,1}^{(1)}\right)^{-1} T^\dagger (Z_M X_1 Z_2 + X_1) T U_{M,1}^{(1)} X_1
\tag{B.40}
$$

$$
= X_2 - Z_1 X_2 Z_3 = h_2^{(1)}.
\tag{B.41}
$$

B.2 Type II

With the construction for Type I phases complete, let us move on to Type II. These are minimally realised with a $\mathbb{Z}_{N_1} \times \mathbb{Z}_{N_2}$ symmetry. The extension from Type I is simple, let the boundary symmetry be realised by

$$
S_{(N_1,N_2)}^{\{1\},(p_1,p_{12})} = \prod_{j=1}^{M} \tau_j^{\{1\}} \prod_{j=1}^{M} U_{j,j+1}^{\{1\},(p_1)} \prod_{j=1}^{M} V_{j,j+2}^{\{1\},(p_{12})},
\tag{B.42}
$$

$$
S_{(N_1,N_2)}^{\{2\},(p_2,p_{21})} = \prod_{j=1}^{M} \tau_j^{\{2\}} \prod_{j=1}^{M} U_{j,j+1}^{\{2\},(p_2)} \prod_{j=1}^{M} V_{j,j+2}^{\{2\},(p_{21})},
\tag{B.43}
$$

where

$$
\left(\tau^{\{a\}}\right)^{N_a} = \left(\sigma^{\{a\}}\right)^{N_a} = \mathbb{1},
\tag{B.44}
$$

$$
\sigma_j^{\{a\}} \tau_k^{\{b\}} = \omega_a^{\delta_{jk}\delta_{ab}} \tau_k^{\{b\}} \sigma_j^{\{a\}},
\tag{B.45}
$$

$$
\omega_a = \exp\left(\frac{2\pi i}{N_a}\right),
\tag{B.46}
$$

$$
U_{j,j+1}^{\{a\},(p_a)} = \exp\left(-\frac{2\pi i}{N_a^2} p_a \left\{ \frac{N_a - 1}{2} + \sum_{x=1}^{N_a-1} \frac{(\sigma_j^{\{a\}\dagger}\sigma_{j+1}^{\{a\}})^x}{\omega_a^x - 1} \right\}\right),
\tag{B.47}
$$

B. 4

$$V_{j,j+2}^{\{a\},(p_{ab})} = \exp\left(-\frac{2\pi i}{N_a N_{ab}} p_{ab} \left\{\frac{N_{ab}-1}{2} + \sum_{x=1}^{N_{ab}-1} \frac{(\tilde{\sigma}_j^{\{b\}\dagger}\tilde{\sigma}_{j+2}^{\{b\}})^x}{\omega_{ab}^x - 1}\right\}\right), \tag{B.48}$$

and

$$N_{ab} = \gcd(N_a, N_b) \tag{B.49}$$

$$\omega_{ab} = \exp\left(\frac{2\pi i}{N_{ab}}\right), \tag{B.50}$$

$$\tilde{\sigma}_j^{\{a\}}\tau_k^{\{b\}} = \omega_{ab}^{\delta_{jk}\delta_{ab}}\tau_k^{\{b\}}\tilde{\sigma}_j^{\{a\}}. \tag{B.51}$$

Here p_1, p_2 are Type I labels, and p_{12}, p_{21} are of Type II. Note that the Type II operators V act on next nearest neighbour sites. This is to prevent cancellation of the Type I parts; if these are not present, the symmetry can be reduced to a nearest neighbour operator. The Hamiltonian ansatz becomes

$$H_{\vec{N}}^{(\vec{p})} = -\lambda \sum_{j=1}^{M} \sum_{\vec{a}=0}^{\vec{N}-1} \left(\vec{S}_{\vec{N}}^{(\vec{p})}\right)^{-\vec{a}} \vec{\tau}_j \left(\vec{S}_{\vec{N}}^{(\vec{p})}\right)^{\vec{a}} + hc \tag{B.52}$$

$$= -\lambda \sum_{j=1}^{M} \sum_{a_1=0}^{N_1-1} \sum_{a_2=0}^{N_2-1} \left(S_{(N_1,N_2)}^{\{1\},(p_1,p_{12})}\right)^{-a_1} \left(S_{(N_1,N_2)}^{\{2\},(p_2,p_{21})}\right)^{-a_2} (\tau_j^{\{1\}} + \tau_j^{\{2\}}) \times$$

$$\left(S_{(N_1,N_2)}^{\{1\},(p_1,p_{12})}\right)^{a_1} \left(S_{(N_1,N_2)}^{\{2\},(p_2,p_{21})}\right)^{a_2} + hc. \tag{B.53}$$

From here we will allow the $\vec{A}$ notation to be implied. With this, we can construct explicit Hamiltonians.

B.2.1 $\mathbb{Z}_2 \times \mathbb{Z}_2$ Symmetry

B.2.1.1 Translationally Invariant and Periodic

Since we dealt with the case of Type I indices above, let $p_1 = p_2 = 0$. Let $p_{12} = 1$ to examine the nontrivial phase. It is then sufficient to let $p_{21} = 0$. In this phase, we have the edge symmetry operators (reducing V to a nearest neighbour operator as discussed)

$$S^{\{1\}} = \prod_{j=1}^{M} \tau_j^{\{1\}} \prod_{j=1}^{M} V_{j,j+1}^{\{1\},(1)}, \tag{B.54}$$

$$= \prod_{j=1}^{M} \tau_j^{\{1\}} \prod_{j=1}^{M} \exp\left(-\frac{\pi i}{4}\left\{1 - \tilde{\sigma}_j^{\{2\}\dagger}\tilde{\sigma}_{j+1}^{\{2\}}\right\}\right) \tag{B.55}$$

$$= \exp\left(-\frac{\pi i M}{4}\right) \prod_{j=1}^{M} \tau_j^{\{1\}} \prod_{j=1}^{M} \exp\left(\frac{\pi i}{4}\tilde{\sigma}_j^{\{2\}\dagger}\tilde{\sigma}_{j+1}^{\{2\}}\right) \tag{B.56}$$

$$S^{\{2\}} = \prod_{j=1}^{M} \tau_j^{\{2\}}. \tag{B.57}$$

The Hamiltonian is

$$H = -2\lambda \sum_{j=1}^{M} (X_j^{\{1\}} + X_j^{\{2\}}) +$$

$$\prod_{k=1}^{M} \exp\left(-\frac{\pi i}{4} Z_k^{\{2\}} Z_{k+1}^{\{2\}}\right) (X_j^{\{1\}} + X_j^{\{2\}}) \prod_{k=1}^{M} \exp\left(\frac{\pi i}{4} Z_k^{\{2\}} Z_{k+1}^{\{2\}}\right) \tag{B.58}$$

$$= -2\lambda \sum_{j=1}^{M} (2X_j^{\{1\}} + X_j^{\{2\}}) + \exp\left(-\frac{\pi i}{4} Z_{j-1}^{\{2\}} Z_j^{\{2\}}\right) \exp\left(-\frac{\pi i}{4} Z_j^{\{2\}} Z_{j+1}^{\{2\}}\right) X_j^{\{2\}} \times$$

$$\exp\left(\frac{\pi i}{4} Z_{j-1}^{\{2\}} Z_j^{\{2\}}\right) \exp\left(\frac{\pi i}{4} Z_j^{\{2\}} Z_{j+1}^{\{2\}}\right) \tag{B.59}$$

$$= -2\lambda \sum_{j=1}^{M} (2X_j^{\{1\}} + X_j^{\{2\}}) + \exp\left(-\frac{\pi i}{2} Z_{j-1}^{\{2\}} Z_j^{\{2\}}\right) \exp\left(-\frac{\pi i}{2} Z_j^{\{2\}} Z_{j+1}^{\{2\}}\right) X_j^{\{2\}} \tag{B.60}$$

$$= -2\lambda \sum_{j=1}^{M} (2X_j^{\{1\}} + X_j^{\{2\}} - Z_{j-1}^{\{2\}} X_j^{\{2\}} Z_{j+1}^{\{2\}}). \tag{B.61}$$

This is simply a gapped chain (subspace 1) and a gapless chain (subspace 2) with $c = 1$ as before.

B.2.1.2 Twisted Boundary Conditions

We define the twisted translation operator in the above phase by

$$\tilde{T}^{(p)} = T V_{M,1}^{\{1\},(1)} X_1^{\{1\}}. \tag{B.62}$$

The untwisted Hamiltonian is given by

$$H = -2\lambda \sum_{j=1}^{M} (2X_j^{\{1\}} + X_j^{\{2\}} - Z_{j-1}^{\{2\}} X_j^{\{2\}} Z_{j+1}^{\{2\}}). \tag{B.63}$$

$$= -2\lambda \sum_{j=1}^{M} h_j. \tag{B.64}$$

As above, we can see that most terms will remain unchanged when the new translation operator is introduced. We compute the terms that are changed

$$\tilde{h}_M = \left(X_1^{\{1\}}\right)^{\dagger} \left(V_{M,1}^{\{1\},(1)}\right)^{-1} T^{\dagger} (2X_{M-1}^{\{1\}} + X_{M-1}^{\{2\}} - Z_{M-2}^{\{2\}} X_{M-1}^{\{2\}} Z_M^{\{2\}}) T V_{M,1}^{\{1\},(1)} X_1^{\{1\}} \tag{B.65}$$

$$= \exp\left(-\frac{\pi i}{4} Z_M^{\{2\}} Z_1^{\{2\}}\right) (2X_M^{\{1\}} + X_M^{\{2\}} - Z_{M-1}^{\{2\}} X_M^{\{2\}} Z_1^{\{2\}}) \exp\left(\frac{\pi i}{4} Z_M^{\{2\}} Z_1^{\{2\}}\right) \tag{B.66}$$

$$= 2X_M^{\{1\}} + (Y_M^{\{2\}} Z_1^{\{2\}} - Z_{M-1}^{\{2\}} Y_M^{\{2\}}) \tag{B.67}$$

$$\tilde{h}_1 = \exp\left(-\frac{\pi i}{4} Z_M^{\{2\}} Z_1^{\{2\}}\right) (2X_1^{\{1\}} + Y_1^{\{2\}} Z_2^{\{2\}} - Z_M^{\{2\}} Y_1^{\{2\}}) \exp\left(\frac{\pi i}{4} Z_M^{\{2\}} Z_1^{\{2\}}\right) \tag{B.68}$$

$$= 2X_1^{\{1\}} + X_1^{\{2\}} - Z_M^{\{2\}} X_1^{\{2\}} Z_2^{\{2\}} \tag{B.69}$$

$$= h_1, \tag{B.70}$$

so the only term which changes is

$$\tilde{h}_M = 2X_M^{\{1\}} + (Y_M^{\{2\}} Z_1^{\{2\}} - Z_{M-1}^{\{2\}} Y_M^{\{2\}}). \tag{B.71}$$

B.3 Type III

Now we have completed the simplest constructions for Type I and II, we move onto Type III. The extension is nontrivial, unlike that from I→II. For simplicity, let us assume that all non Type III indices are 0, and it is sufficient to allow the only nonzero index to be p_{123}

Suppose we have a bulk SPT protected by $S_{\mathrm{bulk}} = \mathbb{Z}_{N_1} \times \mathbb{Z}_{N_2} \times \mathbb{Z}_{N_3}$. Define $\mathbb{Z}_{N_m}$ variables at site j by

$$\left(\sigma_j^{\{m\}}\right)^{N_m} = \left(\tau_j^{\{m\}}\right)^{N_m} = 1 \tag{B.72}$$

$$\sigma_j^{\{m\}} \tau_n^{\{k\}} = \omega_m^{\delta_{mn}\delta_{jk}} \tau_n^{\{k\}} \sigma_j^{\{m\}}, \tag{B.73}$$

where

$$\omega_m = \exp\left(\frac{2\pi i}{N_m}\right). \tag{B.74}$$

Make the ansatz for the symmetry action on the edge given by

$$S_{N_1}^{\{u\}} = \prod_{j=1}^{M} \tau_j^{\{u\}} \prod_{k=1}^{M} W_{k,k+1;N_u}^{\{u\}}, \tag{B.75}$$

where

$$W_{j,j+1;N_u}^{\{u\}} = \prod_{v,w=1}^{3} \left[\left(\sigma_j^{\{v\}}\right)^\dagger \sigma_{j+1}^{\{v\}}\right]^{\frac{N_v N_w}{i2\pi \gcd(N_u,N_v,N_w)}\epsilon_{uvw}p_{uvw}\log\sigma_j^{\{w\}}}. \tag{B.76}$$

This is a strange operator, so we give an example to make it clear (one can also take this as the definition of the operator). On the Hilbert space $\mathcal{H}^{\{3\}} \otimes \mathcal{H}^{\{2\}}$, we can write it explicitly as

$$\left[\left(\sigma_j^{\{2\}}\right)^\dagger \sigma_{j+1}^{\{2\}}\right]^{\frac{N_2 N_3}{i2\pi N_{123}}p_{123}\log\sigma_j^{\{3\}}} =$$

$$\left(\begin{matrix} \left[\left(\sigma_j^{\{2\}}\right)^\dagger \sigma_{j+1}^{\{2\}}\right]^{\log\omega_3^0} & 0 & \cdots & 0 \\ 0 & \left[\left(\sigma_j^{\{2\}}\right)^\dagger \sigma_{j+1}^{\{2\}}\right]^{\log\omega_3^1} & \cdots & 0 \\ 0 & 0 & \ddots & 0 \\ 0 & 0 & \cdots & \left[\left(\sigma_j^{\{2\}}\right)^\dagger \sigma_{j+1}^{\{2\}}\right]^{\log\omega_3^{(N_3-1)}} \end{matrix}\right)_j^{\frac{N_2 N_3}{i2\pi N_{123}}p_{123}} \tag{B.77}$$

$$= \left(\begin{matrix} \left[\left(\sigma_j^{\{2\}}\right)^\dagger \sigma_{j+1}^{\{2\}}\right]^0 & 0 & \cdots & 0 \\ 0 & \left[\left(\sigma_j^{\{2\}}\right)^\dagger \sigma_{j+1}^{\{2\}}\right]^1 & \cdots & 0 \\ 0 & 0 & \ddots & 0 \\ 0 & 0 & \cdots & \left[\left(\sigma_j^{\{2\}}\right)^\dagger \sigma_{j+1}^{\{2\}}\right]^{N_3-1} \end{matrix}\right)_j^{\frac{N_2}{N_{123}p_{123}}}. \tag{B.78}$$

B.3.1 $\mathbb{Z}_2 \times \mathbb{Z}_2 \times \mathbb{Z}_2$ Symmetry

B.3.1.1 Translationally Invariant and Periodic

Let us now specialise to the case of $\mathbb{Z}_2 \times \mathbb{Z}_2 \times \mathbb{Z}_2$ symmetry in the bulk. Pick the phase labelled by $p_\alpha = 0$ for $\alpha \neq 123$ and $p_{123} = 1$. In this phase, we end up with the boundary symmetry operators

$$S_2^{\{1\}} = \prod_{j=1}^{M} X_j^{\{1\}} \prod_{j=1}^{M} \left[Z_j^{\{2\}} Z_{j+1}^{\{2\}} \right]^{\frac{\log Z_j^{\{3\}}}{i\pi}}, \tag{B.79}$$

$$S_2^{\{2\}} = \prod_{j=1}^{M} X_j^{\{2\}}, \tag{B.80}$$

$$S_2^{\{3\}} = \prod_{j=1}^{M} X_j^{\{3\}}, \tag{B.81}$$

The ansatz Hamiltonian for this phase is therefore

$$H = -4 \sum_{j=1}^{M} (X_j^{\{1\}} + X_j^{\{2\}} + X_j^{\{3\}}) + \left(S_2^{\{1\}} \right)^{-1} (X_j^{\{1\}} + X_j^{\{2\}} + X_j^{\{3\}}) \left(S_2^{\{1\}} \right) \tag{B.82}$$

$$= -4 \sum_{j=1}^{M} (X_j^{\{1\}} + X_j^{\{2\}} + X_j^{\{3\}}) + \prod_{k=1}^{M} \left[Z_k^{\{2\}} Z_{k+1}^{\{2\}} \right]^{-\frac{\log Z_k^{\{3\}}}{i\pi}} \times$$

$$(X_j^{\{1\}} + X_j^{\{2\}} + X_j^{\{3\}}) \prod_{k=1}^{M} \left[Z_k^{\{2\}} Z_{k+1}^{\{2\}} \right]^{\frac{\log Z_k^{\{3\}}}{i\pi}} \tag{B.83}$$

$$= -4 \sum_{j=1}^{M} (2X_j^{\{1\}} + X_j^{\{2\}} + X_j^{\{3\}}) + \left[Z_{j-1}^{\{2\}} Z_j^{\{2\}} \right]^{-\frac{\log Z_{j-1}^{\{3\}}}{i\pi}} \left[Z_j^{\{2\}} Z_{j+1}^{\{2\}} \right]^{-\frac{\log Z_j^{\{3\}}}{i\pi}} \times$$

$$(X_j^{\{2\}} + X_j^{\{3\}}) \left[Z_j^{\{2\}} Z_{j+1}^{\{2\}} \right]^{\frac{\log Z_j^{\{3\}}}{i\pi}} \left[Z_{j-1}^{\{2\}} Z_j^{\{2\}} \right]^{\frac{\log Z_{j-1}^{\{3\}}}{i\pi}} \tag{B.84}$$

$$= -4 \sum_{j=1}^{M} (2X_j^{\{1\}} + X_j^{\{2\}} + X_j^{\{3\}}) + \left[Z_{j-1}^{\{2\}} Z_j^{\{2\}} \right]^{-\frac{\log Z_{j-1}^{\{3\}}}{i\pi}} \left[Z_j^{\{2\}} Z_{j+1}^{\{2\}} \right]^{-\frac{\log Z_j^{\{3\}}}{i\pi}} \times$$

$$X_j^{\{2\}} \left[Z_j^{\{2\}} Z_{j+1}^{\{2\}} \right]^{\frac{\log Z_j^{\{3\}}}{i\pi}} \left[Z_{j-1}^{\{2\}} Z_j^{\{2\}} \right]^{\frac{\log Z_{j-1}^{\{3\}}}{i\pi}} +$$

$$\left[Z_j^{\{2\}} Z_{j+1}^{\{2\}} \right]^{-\frac{\log Z_j^{\{3\}}}{i\pi}} X_j^{\{3\}} \left[Z_j^{\{2\}} Z_{j+1}^{\{2\}} \right]^{\frac{\log Z_j^{\{3\}}}{i\pi}} \tag{B.85}$$

$$= -4 \sum_{j=1}^{M} (2X_j^{\{1\}} + X_j^{\{2\}} + X_j^{\{3\}}) + \left[Z_{j-1}^{\{2\}} Z_j^{\{2\}} \right]^{-\frac{\log Z_{j-1}^{\{3\}}}{i\pi}} \left[Z_j^{\{2\}} Z_{j+1}^{\{2\}} \right]^{-\frac{\log Z_j^{\{3\}}}{i\pi}} \times$$

$$\left[-Z_j^{\{2\}} Z_{j+1}^{\{2\}} \right]^{\frac{\log Z_j^{\{3\}}}{i\pi}} \left[-Z_{j-1}^{\{2\}} Z_j^{\{2\}} \right]^{\frac{\log Z_{j-1}^{\{3\}}}{i\pi}} X_j^{\{2\}} + \left[Z_j^{\{2\}} Z_{j+1}^{\{2\}} \right]^{-\frac{\log Z_j^{\{3\}}}{i\pi} + \frac{\log(-Z_j^{\{3\}})}{i\pi}} X_j^{\{3\}} \tag{B.86}$$

$$= -4 \sum_{j=1}^{M} (2X_j^{\{1\}} + X_j^{\{2\}} + X_j^{\{3\}}) + \left[Z_{j-1}^{\{2\}} Z_j^{\{2\}} \right]^{-\frac{\log Z_{j-1}^{\{3\}}}{i\pi}} \left[Z_j^{\{2\}} Z_{j+1}^{\{2\}} \right]^{-\frac{\log Z_j^{\{3\}}}{i\pi}} \times$$

$$\left[-Z_j^{\{2\}}Z_{j+1}^{\{2\}}\right]^{\frac{\log Z_j^{\{3\}}}{i\pi}}\left[-Z_{j-1}^{\{2\}}Z_j^{\{2\}}\right]^{\frac{\log Z_{j-1}^{\{3\}}}{i\pi}}X_j^{\{2\}}+\left[Z_j^{\{2\}}Z_{j+1}^{\{2\}}\right]^{\frac{\log(-1)}{i\pi}}X_j^{\{3\}} \tag{B.87}$$

$$=-4\sum_{j=1}^{M}(2X_j^{\{1\}}+X_j^{\{2\}}+X_j^{\{3\}})+(-1)^{\frac{\log Z_j^{\{3\}}}{i\pi}}(-1)^{\frac{\log Z_{j-1}^{\{3\}}}{i\pi}}X_j^{\{2\}}+Z_j^{\{2\}}X_j^{\{3\}}Z_{j+1}^{\{2\}} \tag{B.88}$$

$$=-4\sum_{j=1}^{M}(2X_j^{\{1\}}+X_j^{\{2\}}+X_j^{\{3\}})+Z_{j-1}^{\{3\}}X_j^{\{2\}}Z_j^{\{3\}}+Z_j^{\{2\}}X_j^{\{3\}}Z_{j+1}^{\{2\}}. \tag{B.89}$$

Identifying the 2 and 3 subspaces as odd and even sites on a single chain, we get

$$H_{\text{TypeIII}}\equiv-8\sum_{j=1}^{M}X_j^{\{1\}}-4\sum_{j=1}^{2M}\tilde{X}_j+\tilde{Z}_{j-1}\tilde{X}_j\tilde{Z}_{j+1}, \tag{B.90}$$

which can be compared to the Type II Hamiltonian

$$H_{\text{TypeII}}=-2\sum_{j=1}^{M}(2X_j^{\{1\}}+X_j^{\{2\}}-Z_{j-1}^{\{2\}}X_j^{\{2\}}Z_{j+1}^{\{2\}}). \tag{B.91}$$

B.3.1.2 Twisted Boundary Conditions

We define the twisted translation operator in the above phase by

$$\tilde{T}^{(p)}=TW_{M,1}^{\{1\},(1)}X_1^{\{1\}}. \tag{B.92}$$

As before, we compute the terms which might change.

$$\tilde{h}_M=\left(X_1^{\{1\}}\right)\left(W_{M,1}^{\{1\},(1)}\right)^{-1}T^\dagger(2X_{M-1}^{\{1\}}+X_{M-1}^{\{2\}}+X_{M-1}^{\{3\}}$$
$$+Z_{M-2}^{\{3\}}X_{M-1}^{\{2\}}Z_{M-1}^{\{3\}}+Z_{M-1}^{\{2\}}X_{M-1}^{\{3\}}Z_M^{\{2\}})TW_{M,1}^{\{1\},(1)}X_1^{\{1\}} \tag{B.93}$$

$$=2X_M^{\{1\}}+\left[Z_M^{\{2\}}Z_1^{\{2\}}\right]^{-\frac{\log Z_M^{\{3\}}}{i\pi}}(X_M^{\{2\}}+X_M^{\{3\}}+$$

$$Z_{M-1}^{\{3\}}X_M^{\{2\}}Z_M^{\{3\}}+Z_M^{\{2\}}X_M^{\{3\}}Z_1^{\{2\}})\left[Z_M^{\{2\}}Z_1^{\{2\}}\right]^{\frac{\log Z_M^{\{3\}}}{i\pi}} \tag{B.94}$$

$$=2X_M^{\{1\}}+\left[Z_M^{\{2\}}Z_1^{\{2\}}\right]^{-\frac{\log Z_M^{\{3\}}}{i\pi}}(X_M^{\{2\}}+Z_{M-1}^{\{3\}}X_M^{\{2\}}Z_M^{\{3\}})\left[Z_M^{\{2\}}Z_1^{\{2\}}\right]^{\frac{\log Z_M^{\{3\}}}{i\pi}}$$

$$+\left[Z_M^{\{2\}}Z_1^{\{2\}}\right]^{-\frac{\log Z_M^{\{3\}}}{i\pi}}(X_M^{\{3\}}+Z_M^{\{2\}}X_M^{\{3\}}Z_1^{\{2\}})\left[Z_M^{\{2\}}Z_1^{\{2\}}\right]^{\frac{\log Z_M^{\{3\}}}{i\pi}} \tag{B.95}$$

$$=2X_M^{\{1\}}+\left[Z_M^{\{2\}}Z_1^{\{2\}}\right]^{-\frac{\log Z_M^{\{3\}}}{i\pi}}\left[-Z_M^{\{2\}}Z_1^{\{2\}}\right]^{\frac{\log Z_M^{\{3\}}}{i\pi}}(X_M^{\{2\}}+Z_{M-1}^{\{3\}}X_M^{\{2\}}Z_M^{\{3\}})$$

$$+\left[Z_M^{\{2\}}Z_1^{\{2\}}\right]^{-\frac{\log Z_M^{\{3\}}}{i\pi}}\left[Z_M^{\{2\}}Z_1^{\{2\}}\right]^{\frac{\log(-Z_M^{\{3\}})}{i\pi}}(X_M^{\{3\}}+Z_M^{\{2\}}X_M^{\{3\}}Z_1^{\{2\}}) \tag{B.96}$$

$$=2X_M^{\{1\}}+(-1)^{\frac{\log Z_M^{\{3\}}}{i\pi}}(X_M^{\{2\}}+Z_{M-1}^{\{3\}}X_M^{\{2\}}Z_M^{\{3\}})$$

$$+\left[Z_M^{\{2\}}Z_1^{\{2\}}\right]^{\frac{\log(-1)}{i\pi}}(X_M^{\{3\}}+Z_M^{\{2\}}X_M^{\{3\}}Z_1^{\{2\}}) \tag{B.97}$$

$$=2X_M^{\{1\}}+X_M^{\{2\}}Z_M^{\{3\}}+Z_{M-1}^{\{3\}}X_M^{\{2\}}+Z_M^{\{2\}}X_M^{\{3\}}Z_1^{\{2\}}+X_M^{\{3\}} \tag{B.98}$$

$$\tilde{h}_1 = X_1^{\{1\}} \left(W_{M,1}^{\{1\},(1)}\right)^{-1} T^{\dagger}(2X_M^{\{1\}} + X_M^{\{3\}} + X_M^{\{2\}}Z_M^{\{3\}} +$$

$$Z_{M-1}^{\{3\}}X_M^{\{2\}} + Z_M^{\{2\}}X_M^{\{3\}}Z_1^{\{2\}})TW_{M,1}^{\{1\},(1)}X_1^{\{1\}} \tag{B.99}$$

$$= 2X_1^{\{1\}} + X_1^{\{3\}} + Z_1^{\{2\}}X_1^{\{3\}}Z_2^{\{2\}} + \left[Z_M^{\{2\}}Z_1^{\{2\}}\right]^{-\frac{\log Z_M^{\{3\}}}{i\pi}} (X_1^{\{2\}}Z_1^{\{3\}} +$$

$$Z_M^{\{3\}}X_1^{\{2\}}) \left[Z_M^{\{2\}}Z_1^{\{2\}}\right]^{\frac{\log Z_M^{\{3\}}}{i\pi}} \tag{B.100}$$

$$= 2X_1^{\{1\}} + X_1^{\{3\}} + Z_1^{\{2\}}X_1^{\{3\}}Z_2^{\{2\}} + (-1)^{\frac{\log Z_M^{\{3\}}}{i\pi}}(X_1^{\{2\}}Z_1^{\{3\}} + Z_M^{\{3\}}X_1^{\{2\}}) \tag{B.101}$$

$$= 2X_1^{\{1\}} + X_1^{\{2\}} + X_1^{\{3\}} + Z_1^{\{2\}}X_1^{\{3\}}Z_2^{\{2\}} + Z_M^{\{3\}}X_1^{\{2\}}Z_1^{\{3\}} \tag{B.102}$$

$$= h_j. \tag{B.103}$$

Thus, we have the Type III Hamiltonian for $\mathbb{Z}_2 \times \mathbb{Z}_2 \times \mathbb{Z}_2$ with a gauge flux.